Pyroclastic Density Currents

Overview, Processes, Outlook

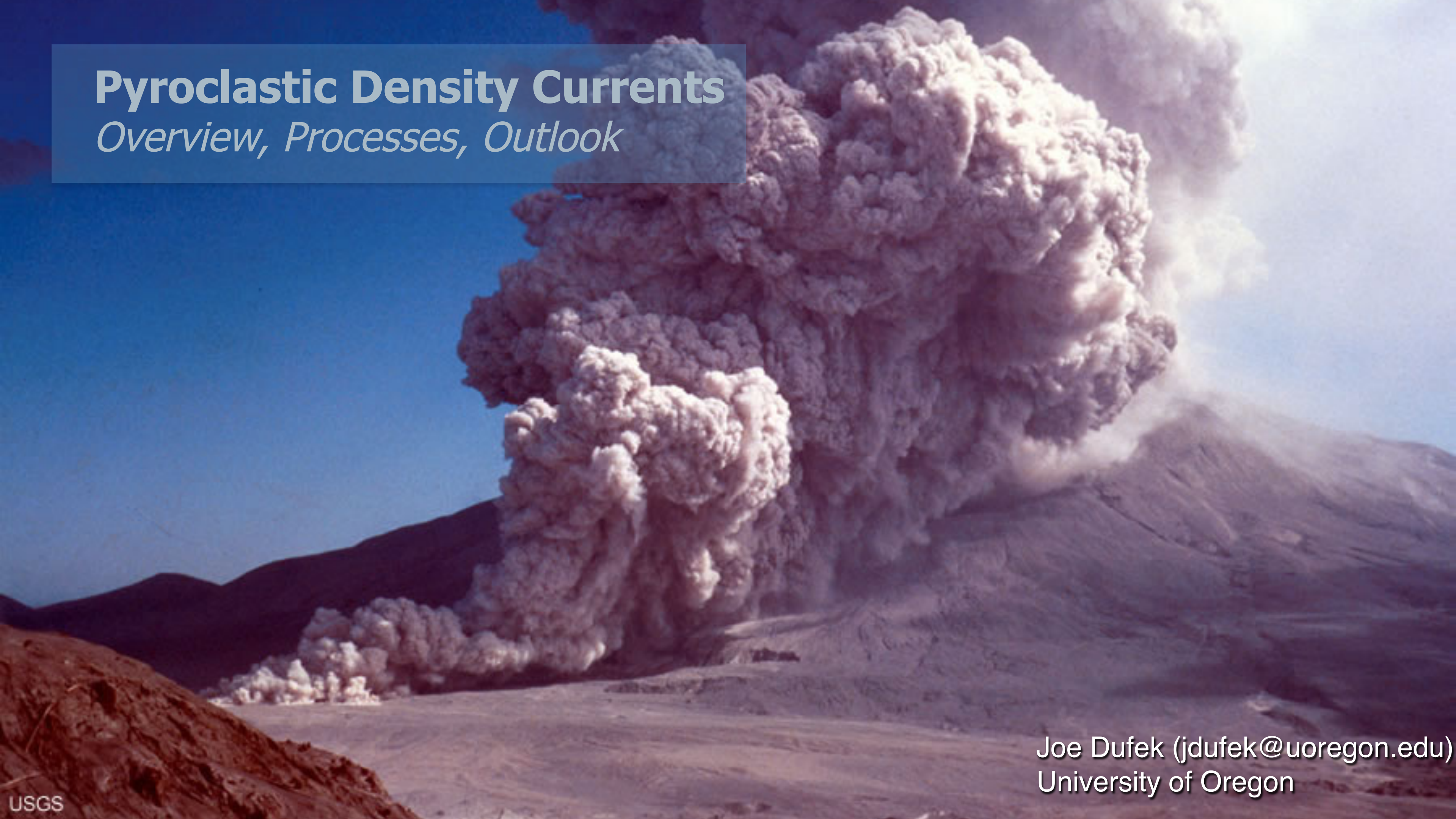

Joe Dufek (jdufek@uoregon.edu)
University of Oregon

Pyroclastic Density Currents

Overview, Processes, Outlook

Special thanks to Gert Lube, Ben Andrews and Olivier Roche

USGS

Joe Dufek (jdufek@uoregon.edu)
University of Oregon

Pyroclastic Density Currents (PDC): Hot, eruption-derived mixture of particles and gas, that moves laterally along the ground, driven by negative buoyancy.

Pyroclastic Surges: Typically used to denote dilute flows.

Pyroclastic Flows: Typically used to denote concentrated flows.

Pyroclastic Gravity Flows

Incandescent Tuff Flows

Ash Flows

Glutwolken

Nuees Ardentes

Sand Flows

Throughout the literature, however, an ever-increasing diversity and duplication in terminology has been used to describe ash-flow materials, and to designate different origins, owing in part to the development of criteria for recognition, and in part to the evolution of ideas on their origin. -- Ross and Smith, 1961

Terminology Evolution *(roughly through time)*

Outline

1. General features of PDC, observations, and historical context.

2. Classical experiments in gravity currents and granular flows.

3. Progress toward a comprehensive conceptual model.

4. Revealing fluid-particle interactions through granular and turbulent experiments.

5. Models of PDC and experiment-model interaction, and internal PDC structure.

6. Open questions and research directions.

Particle Laden Gravity Currents

PDC– Mt. St. Helens

Volcanic Eruption - Io

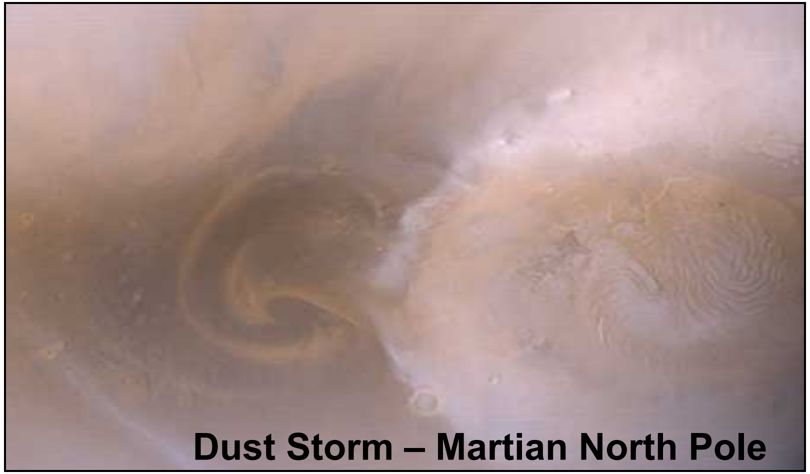

Dust Storm – Martian North Pole

Snow Avalance - Rockies

St. Pierre, Martinique --- Before and after eruption of Mt. Pelee in 1902

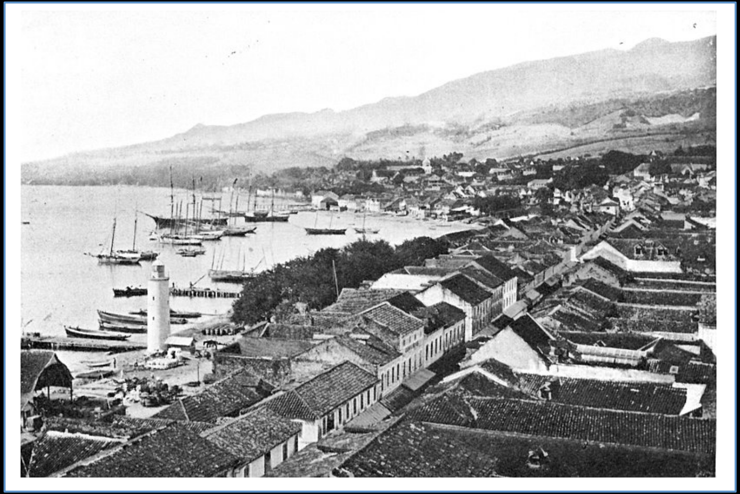

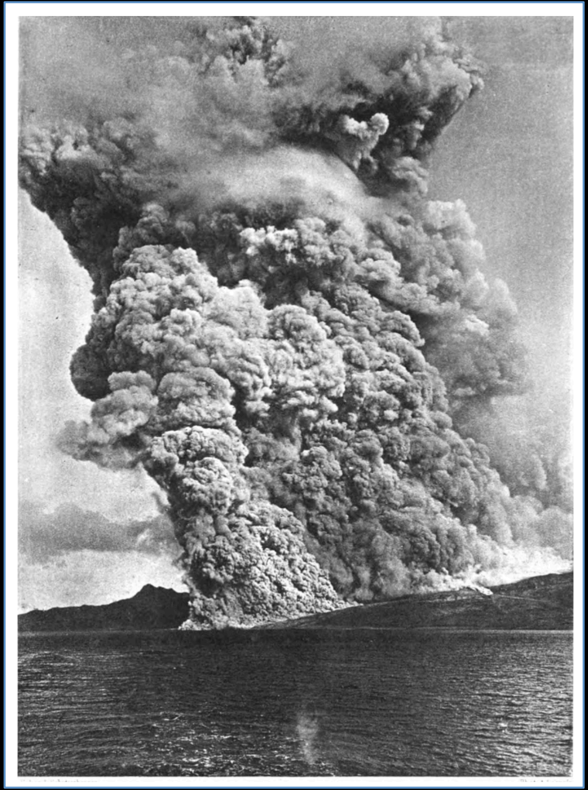

Later PDC (not the same event that caused the damage to the left)

LaCroix, 1904

At the base [of the flow] is found a zone at very high temperature, in which the solid materials predominate (blocks of all dimensions, very small fragments, fine cinders) ; each of these pieces, or the solid particles of which it is formed, radiate heat, and must be surrounded by an atmosphere of gas and vapors, extremely compressed at the beginning, but expanding rapidly; it is this atmosphere which prevents the solid particles from touching one another, maintaining the mass in a state of mobility which allows it to flow over the slope almost in the manner of a liquid.

LaCroix, 1904

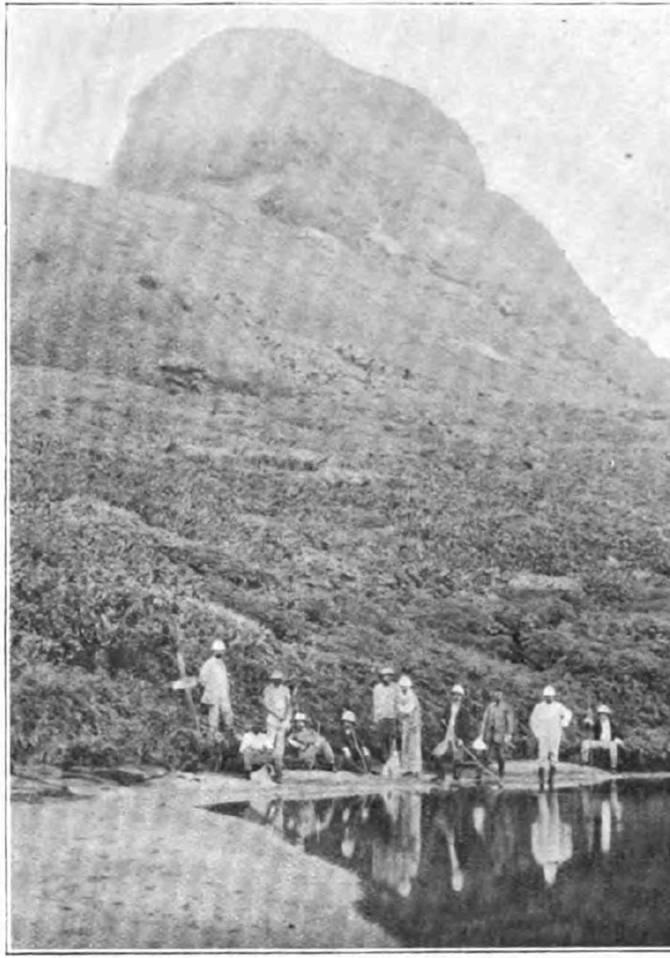

Fig. 3. — Le morne La Croix et le bord occidental du lac des Palmistes avant l'éruption.

PDC generation mechanisms

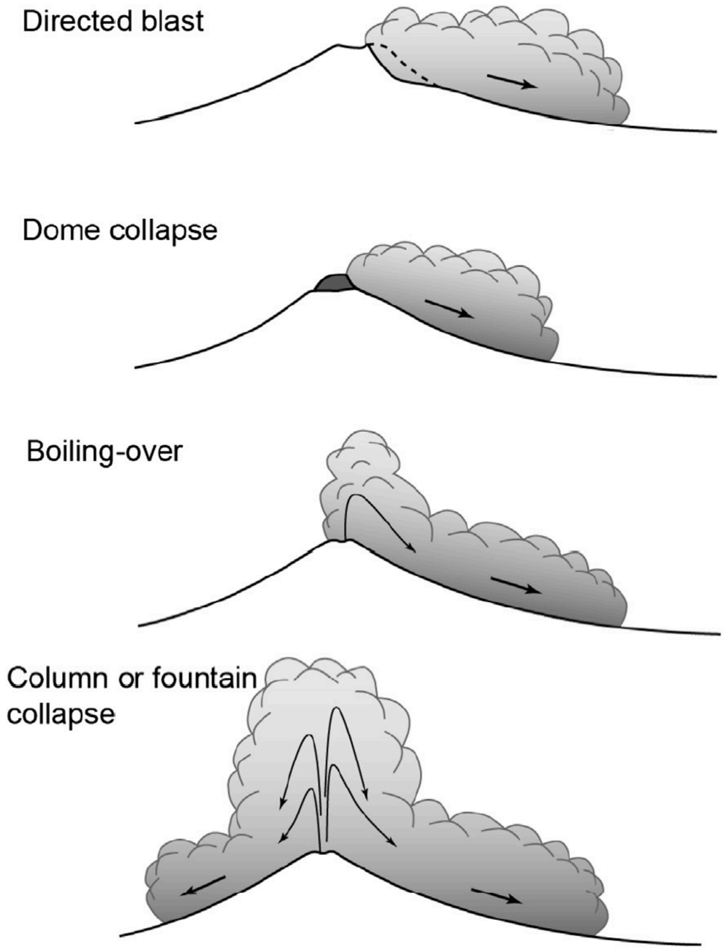

Due to the hazard, opacity, and transitory activity, depositional studies are the foundation of the study of PDC.

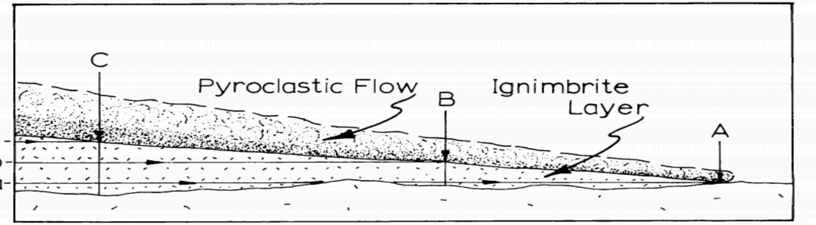

Fig. 9. Diagrammatic illustration of a moving pyroclastic flow and its gradually thickening ignimbrite deposit. Particles along line "a" were deposited from the portion of the flow that has reached station A. Particles along line "b" were deposited from the portion of the flow that has reached station B and so on through innumerable theoretical lines parallel to the base of the deposit deposited by innumerable theoretical turbulent "fronts" that follow the leading edge of the pyroclastic flow.

Fisher, 1966

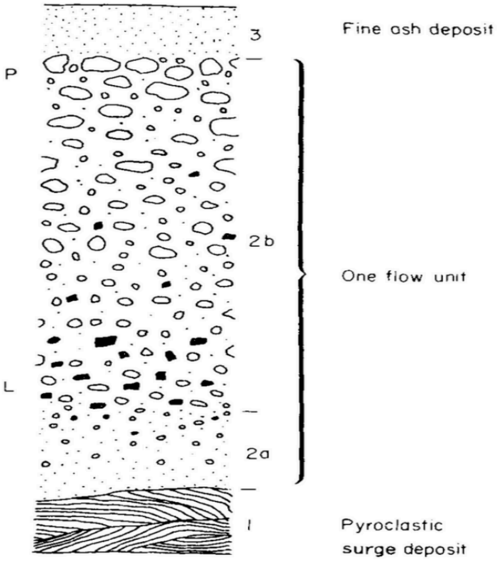

Sparks, Self and Walker, 1973

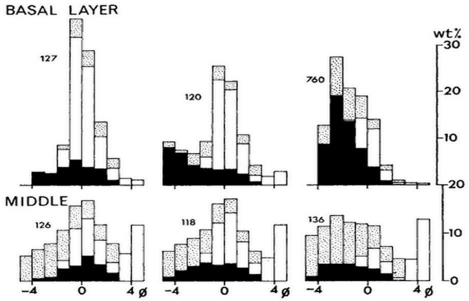

FIG. 12.—Histograms of samples from the basal layer and (*below*) the middle of the same ignimbrite. The bars are subdivided as in fig. 11. Samples 126 and 127 from a pit 1.5 km east of Angra de Heroismo, Terceira, Azores; 118 and 120 from San Mateus shore section, Terceira; and 136 and 760 from Povoacão, São Miguel, Azores.

Walker, 1971

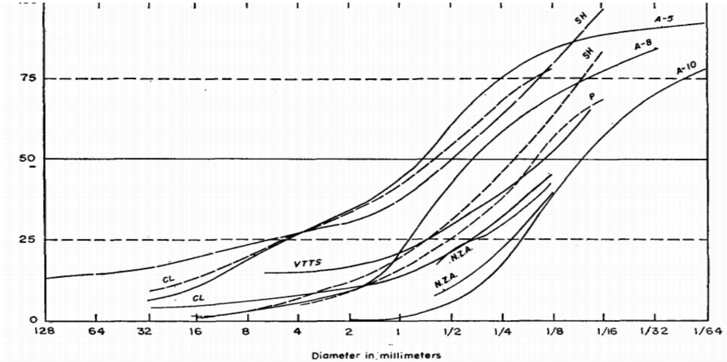

FIGURE 4.—CUMULATIVE CURVES SHOWING SORTING IN ASH FLOWS
SH curves: "Shirasu" deposits, South Kyushu, Japan (Taneda, 1954; 1957; Taneda, Miyachi, and shihara, 1957)
A curves: Asama volcano, Komoro deposits, Japan (Tsuya, Murai, and Hosoya, 1958)
CL curves: "Older pumice," Crater Lake, Oregon (Moore, 1934)
VTTS curve: "Sand flow," Valley of Ten Thousand Smokes, Alaska (Fenner, 1923)
P curve: "Sillar" near Arequipa, Peru (Jenks and Goldich, 1956)
N.Z.A. curve: Nonwelded portion of "ignimbrite," Arapuni, New Zealand (Marshall, 1935)

Smith, 1960

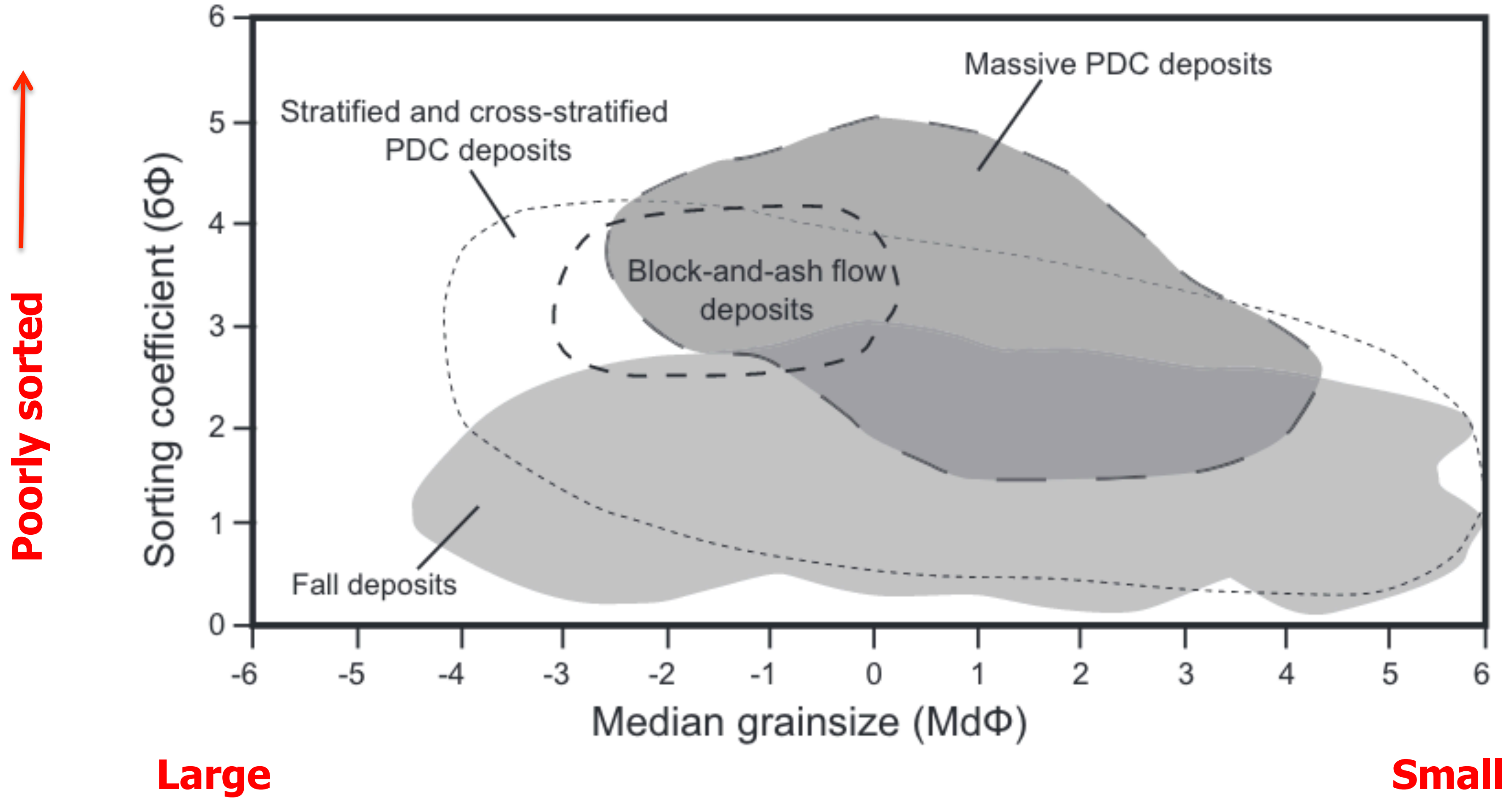

Poorly sorted
Sorting coefficient (6Φ)
6
5
4
3
2
1
0
Massive PDC deposits
Stratified and cross-stratified
PDC deposits
Block-and-ash flow
deposits
Fall deposits
-6
-5
-4
-3
-2
-1
0
1
2
3
4
5
6
Median grainsize (MdΦ)
Large
Small


a
10 μm
b
c
d
e
f

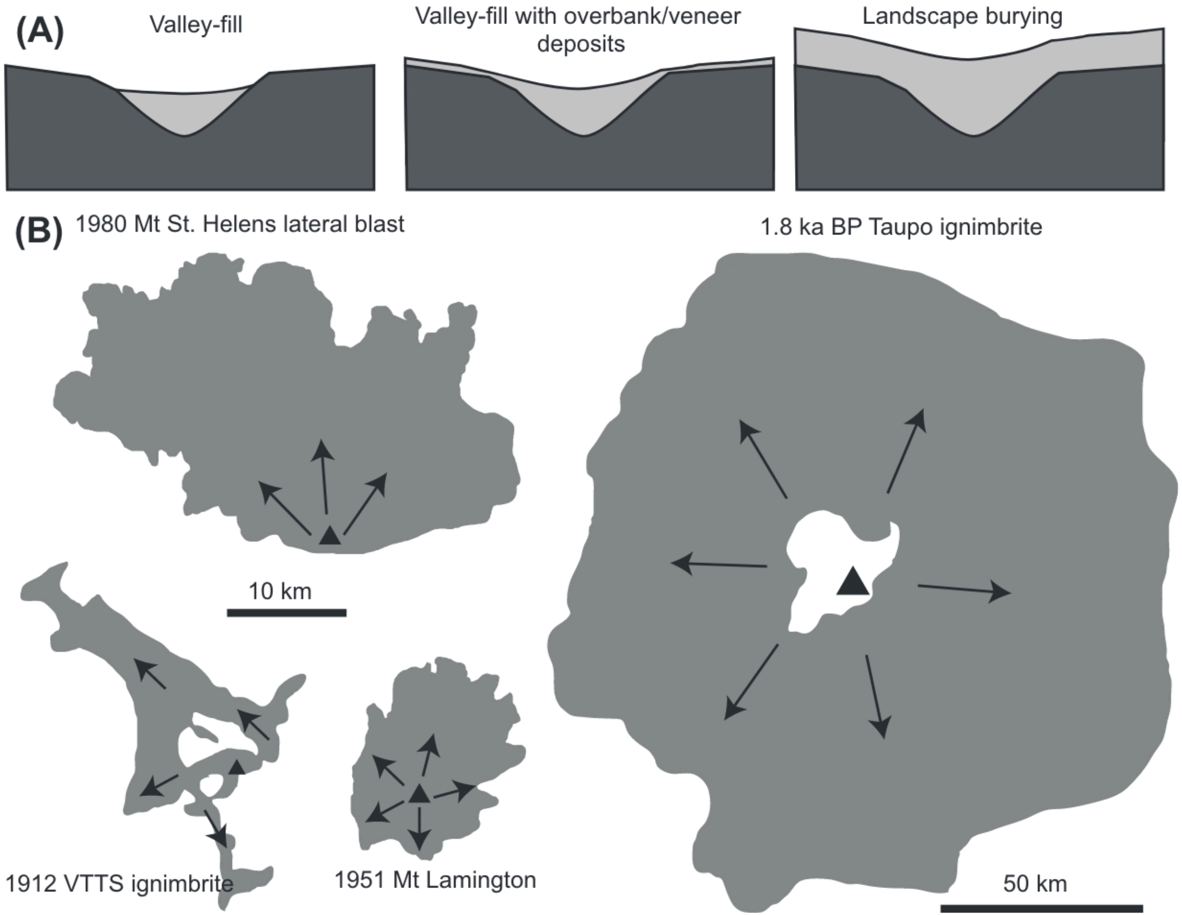

Brown and Andrews, 2015

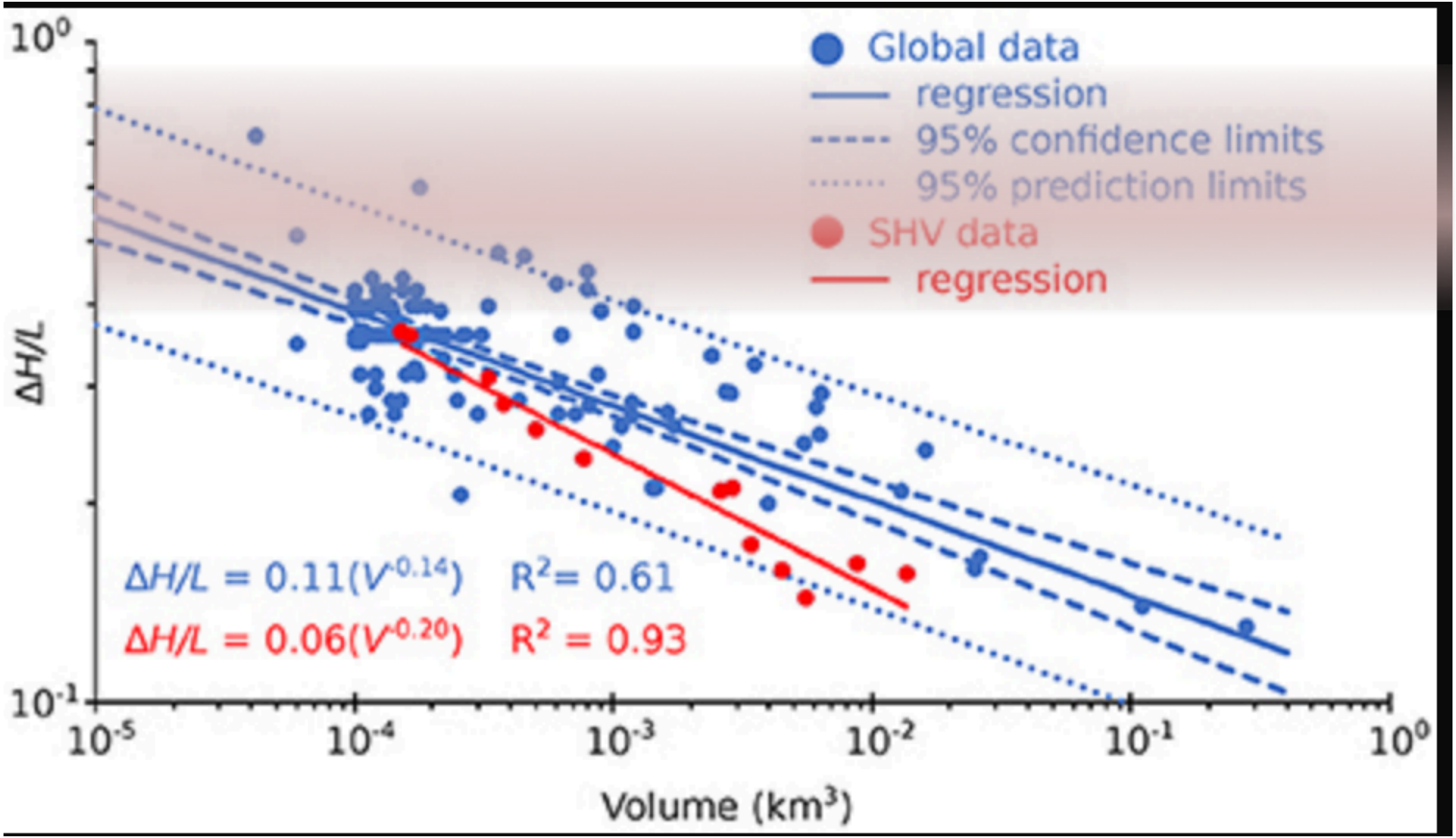
Global data
regression
95% confidence limits
95% prediction limits
SHV data
regression
ΔH/L = 0.11(V^-0.14) R²= 0.61
ΔH/L = 0.06(V^-0.20) R² = 0.93
ΔH/L
Volume (km³)
10^0
10^-1
10^-5
10^-4
10^-3
10^-2
10^-1
10^0

Ogburn, 2012

Enhanced Mobility

A common and highly significant feature of large pyroclastic flows is their ability to surmount considerable topographic barriers. For example, the Ito pyroclastic flow in Japan traveled over barriers of between 400 and 600 m [Yokoyama, 1974]. Pumice flows during the 6000 B.P. eruption of Crater Lake crossed obstacles more than 60 m high [Williams, 1942]. Miller and Smith [1977] have documented pyroclastic flows in Alaska which have also surmounted substantial topographic barriers. The Los Chocoyos ash flow tuff [Koch and McLean, 1974; Rose et al., 1978] is found in low-lying basins in Guatemala separated from the source.

Sparks et al. 1978

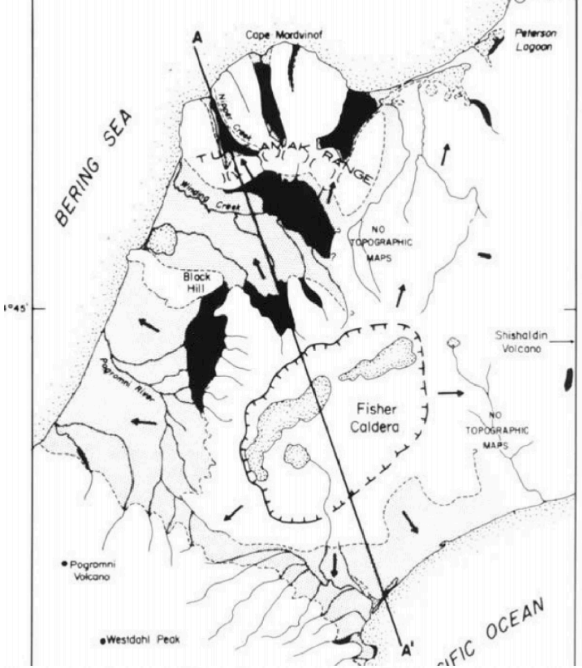

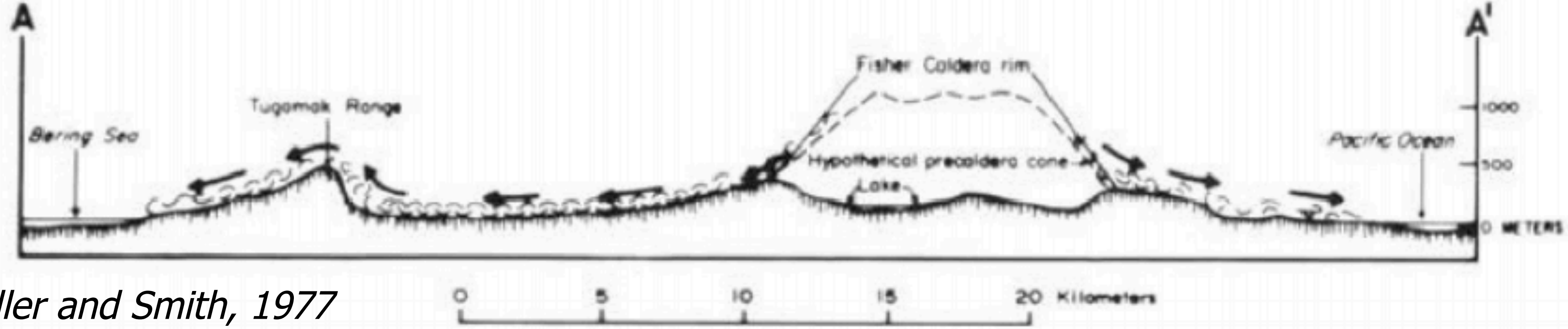

Miller and Smith, 1977

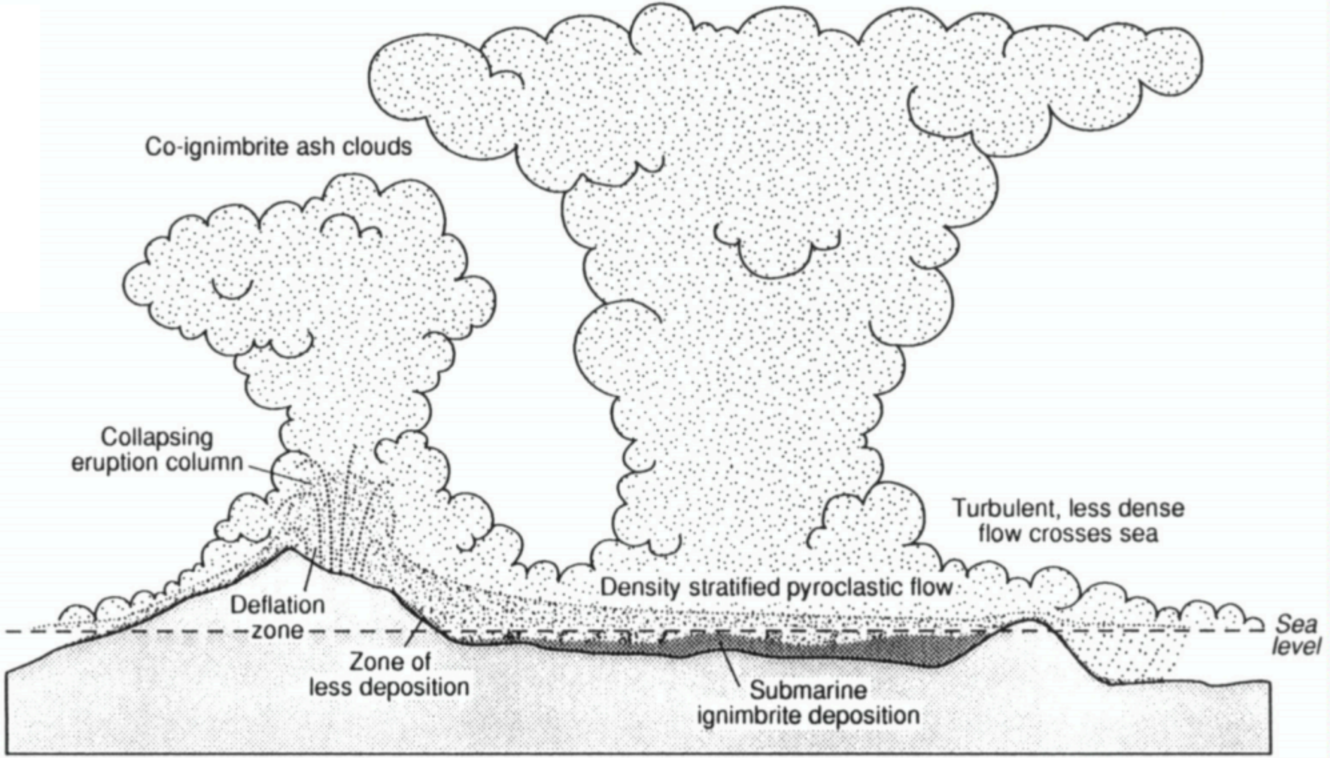

Krakatau, 1883

Self, 1992

Geophysical Observations

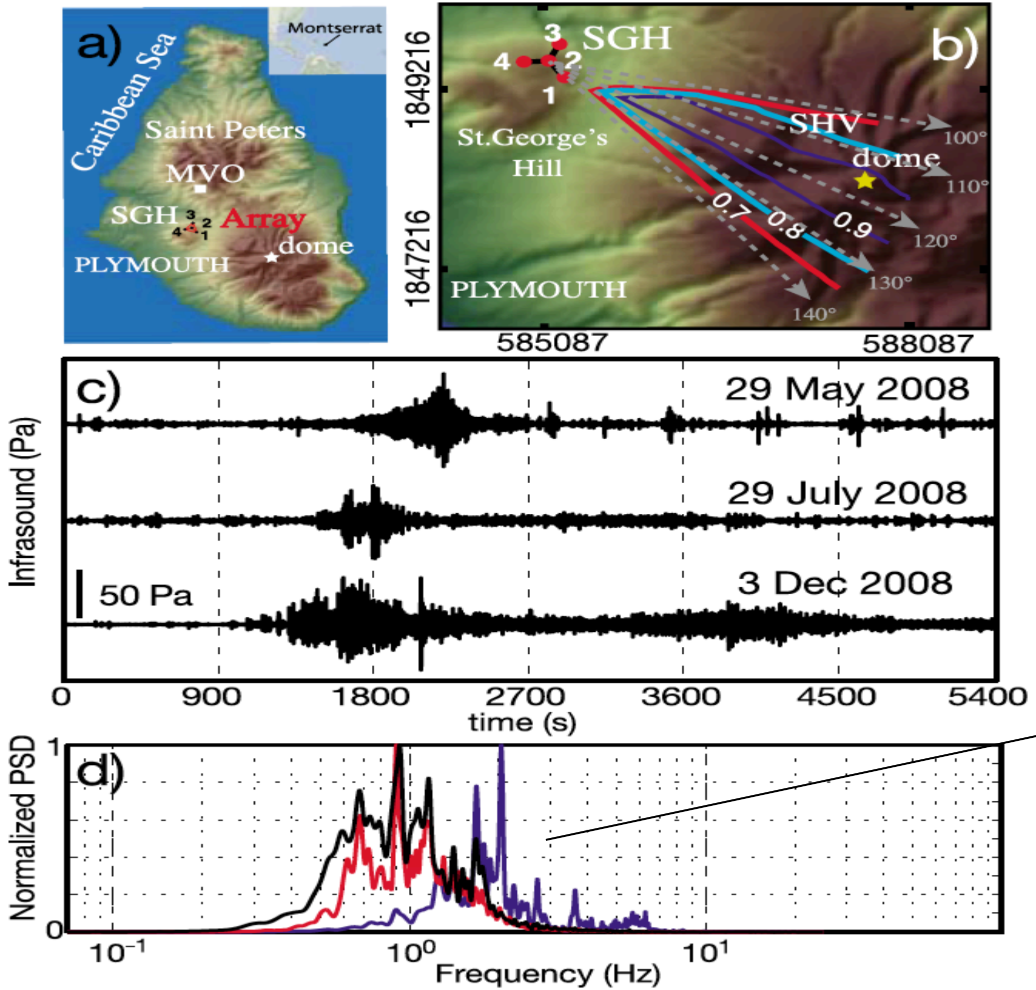

Frequency content may be related to size of flow and component particles

Ripepe et al, 2010

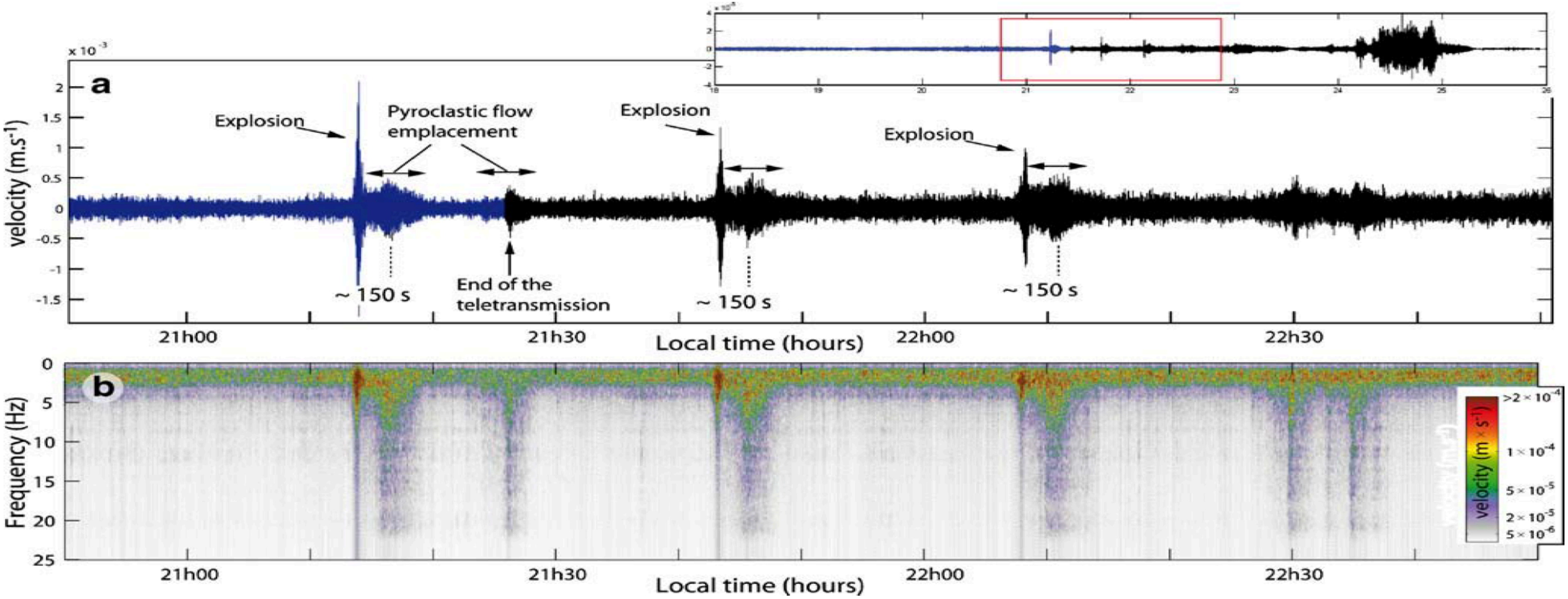

Tungurahua

Kelfoun et al, 2009

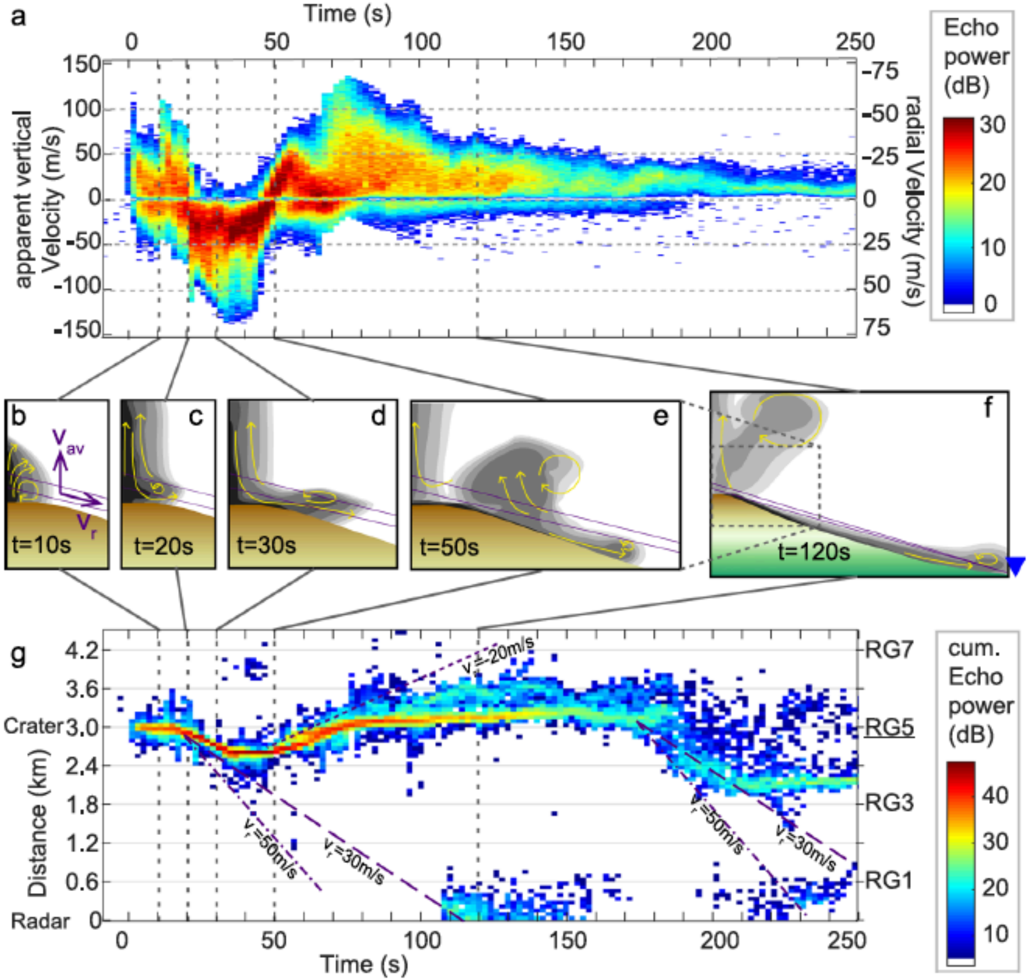

Colima

Scharff et al., 2019

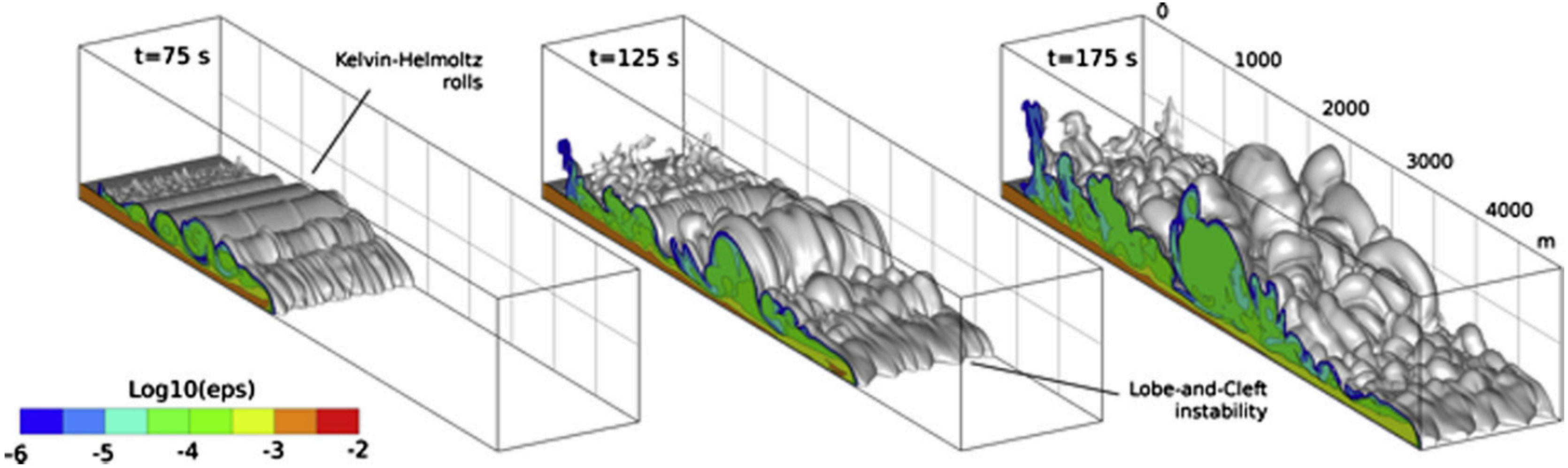
t=75 s
Kelvin-Helmoltz
rolls
t=125 s
t=175 s
0
1000
2000
3000
4000
m
Lobe-and-Cleft
instability
Log10(eps)
-6
-5
-4
-3
-2

Anatomy of ‘classical’ gravity currents, and pyroclastic flow complications

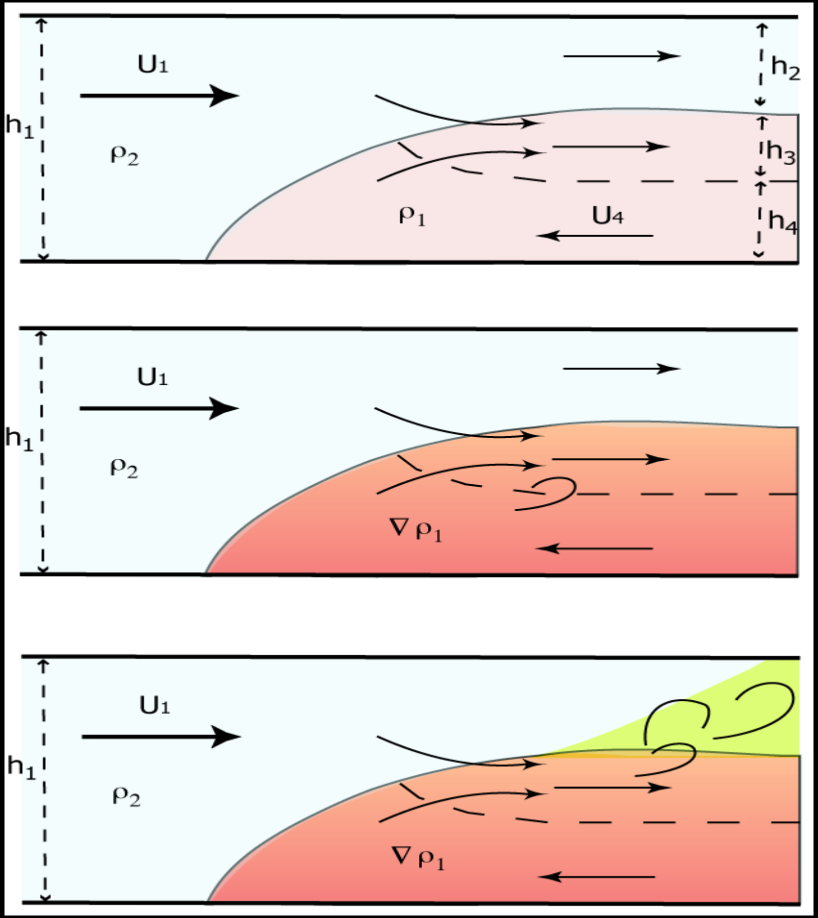

$$Sa = \frac{\rho_p d_p^2 (\partial U / \partial y)^2}{(\rho_p - \rho_f) g H}$$

Collisional stresses relative to frictional stress

Iverson, 1997

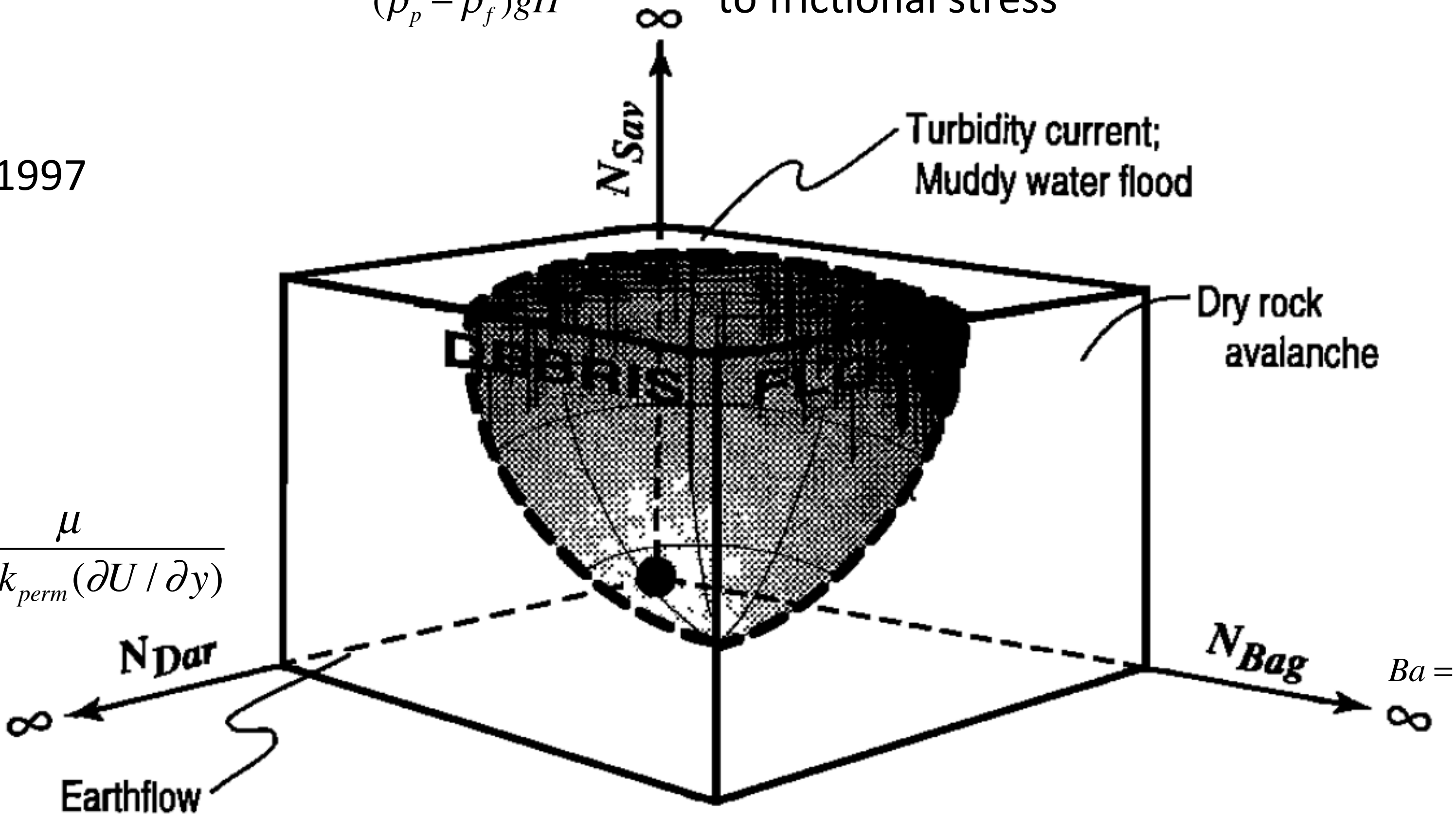

$$Da = \frac{\mu}{\alpha_p \rho_p k_{perm} (\partial U / \partial y)}$$

$$Ba = \frac{\alpha_p \rho_p d_p^2 (\partial U / \partial y}{(1 - \alpha_p) \mu}$$

Fluid drag in porous media relative to collisional stresses

Collisional stresses relative to viscous stresses in fluid

Turbulent Multiphase Flow: Multiple levels of coupling between discrete and continuous phases

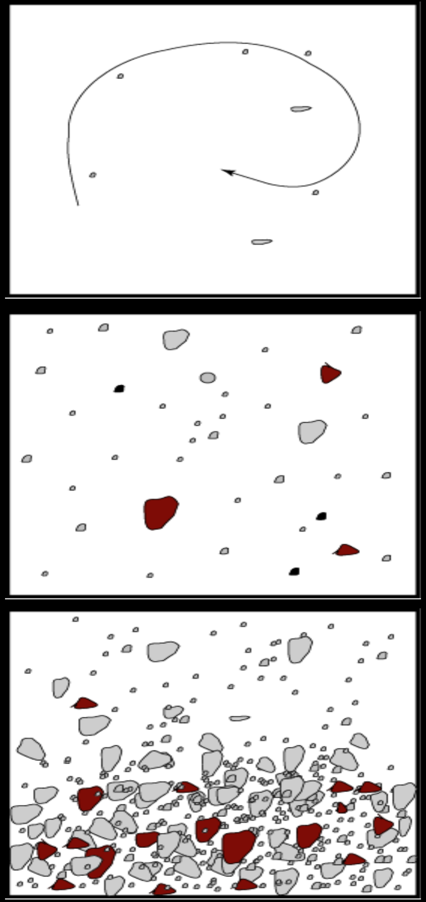

$$D_D = \frac{t_c}{t_p}$$

$$I = \frac{\dot{\gamma} d}{\sqrt{\frac{P_s}{\rho_s}}}$$

Turbulent Multiphase Flow: Multiple levels of coupling between discrete and continuous phases

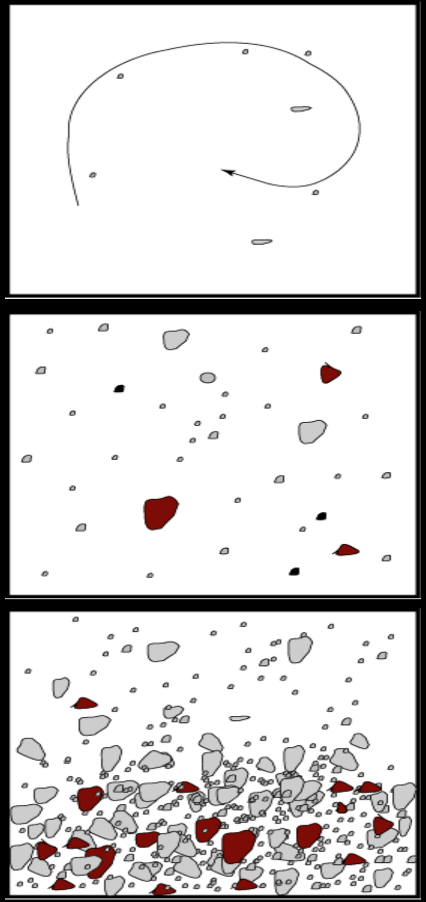

$$I = \frac{\dot{\gamma} d}{\sqrt{\frac{P_s}{\rho_s}}}$$

Inertia Number:

Collisional
$I > 10^{-1}$

Inertial
$10^{-3} - 10^{-1}$

Quasi-static
$I < 10^{-3}$

Fluidization

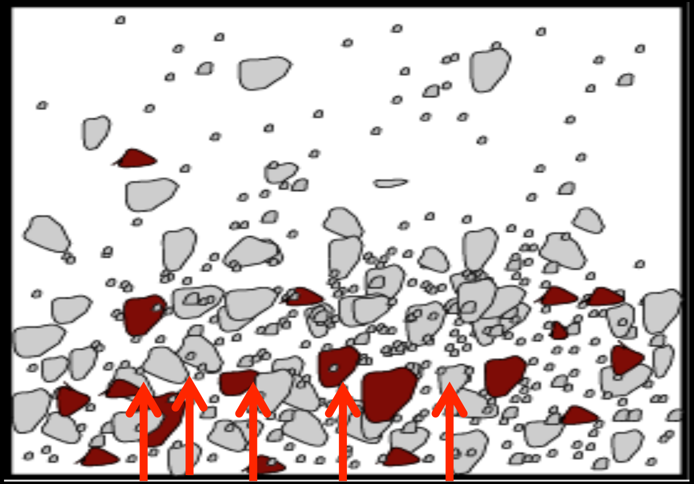

Drag from the upward percolation of gas reduces the normal force and hence friction in a flow.

$$Da = \frac{\mu}{\alpha_p \rho_p k_{perm} (\partial U / \partial y)}$$

Particle/Fluid Interaction in Turbulent Flow

Elghobashi, 1994

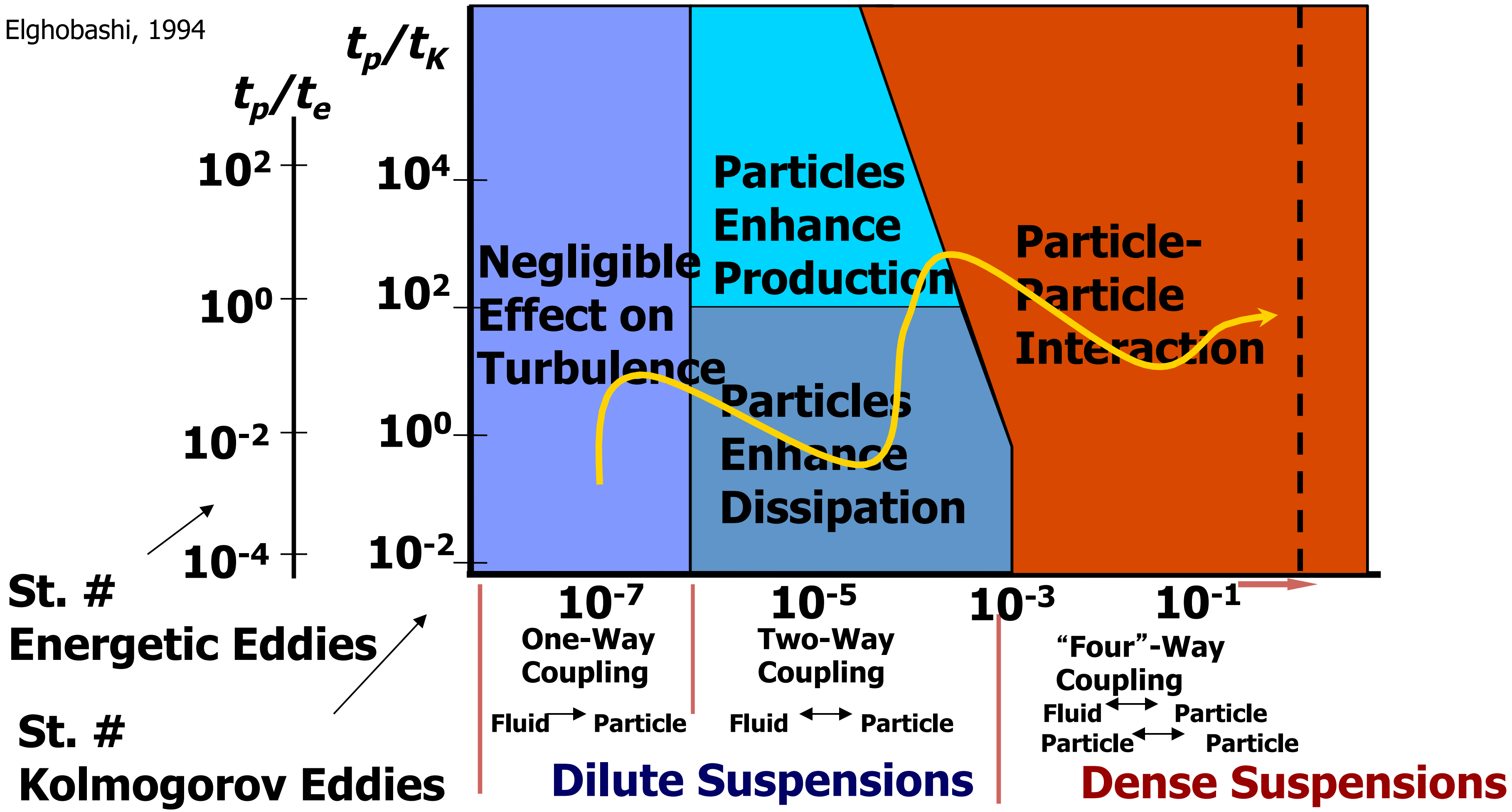

Conceptual Model for PDC

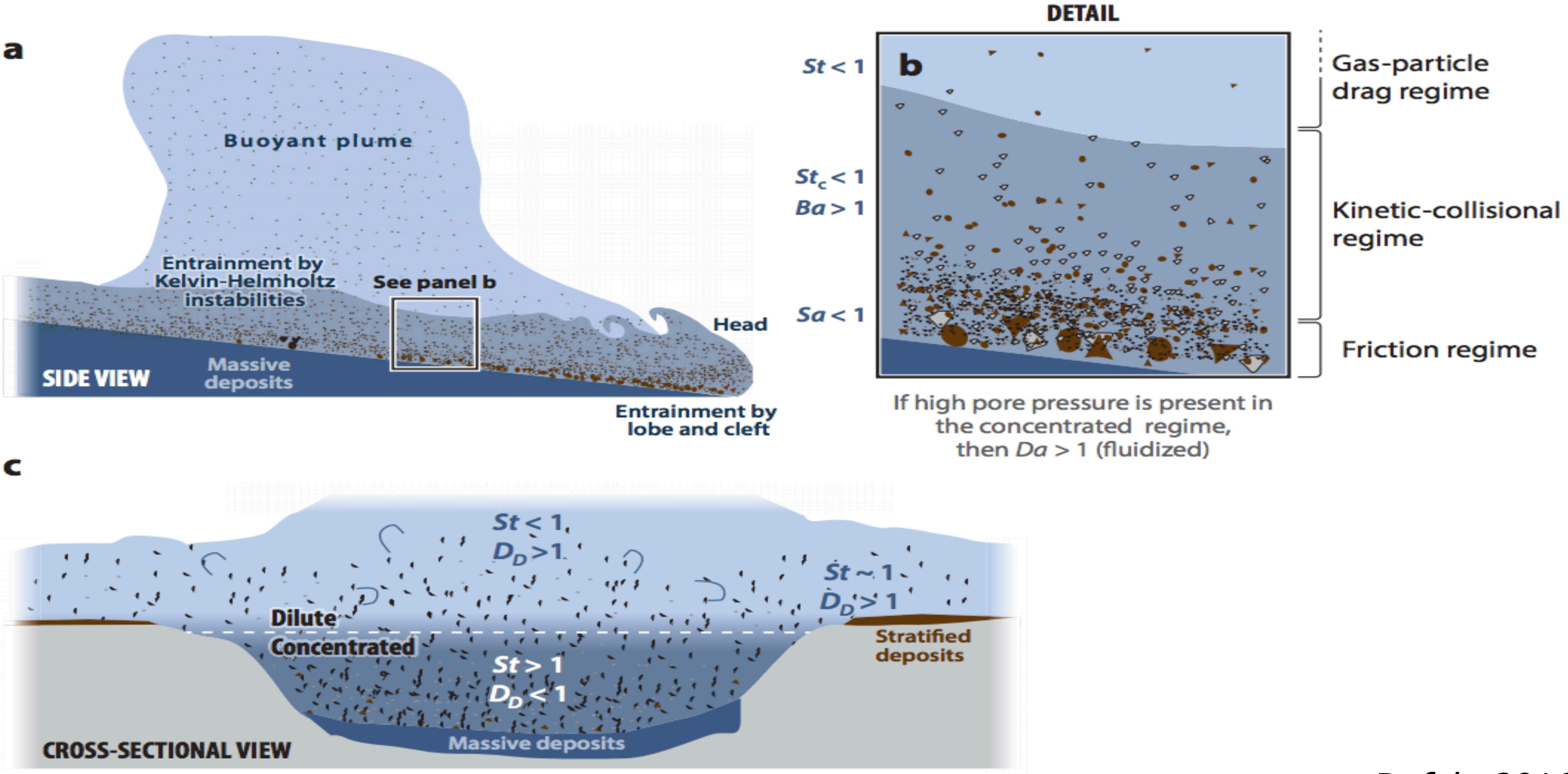

Dufek, 2016

Macroscale Experiments

Fluidized Currents

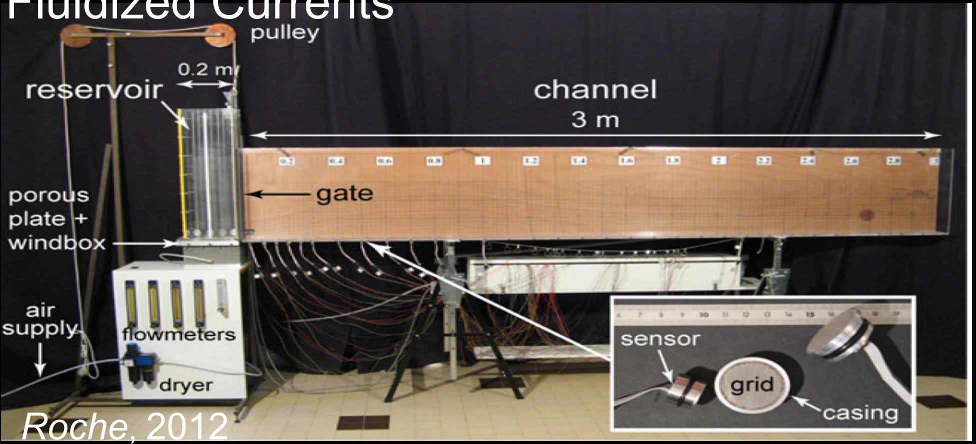

Roche, 2012

Dilute Gravity Currents

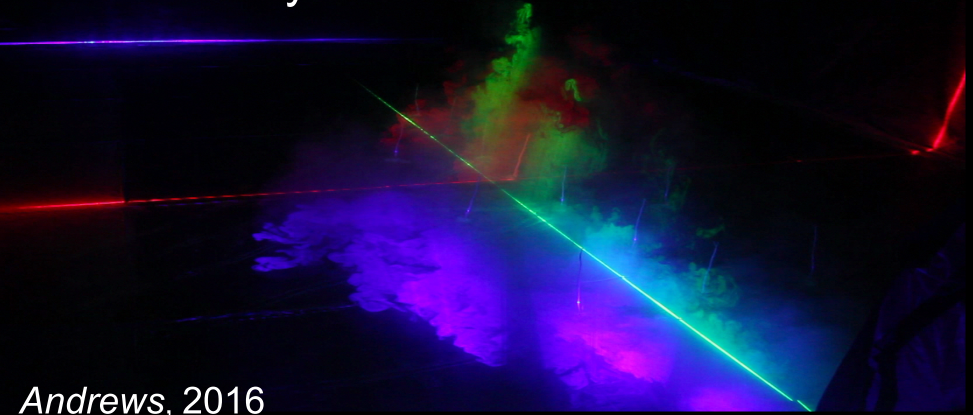

Andrews, 2016

Large Scale Experiments

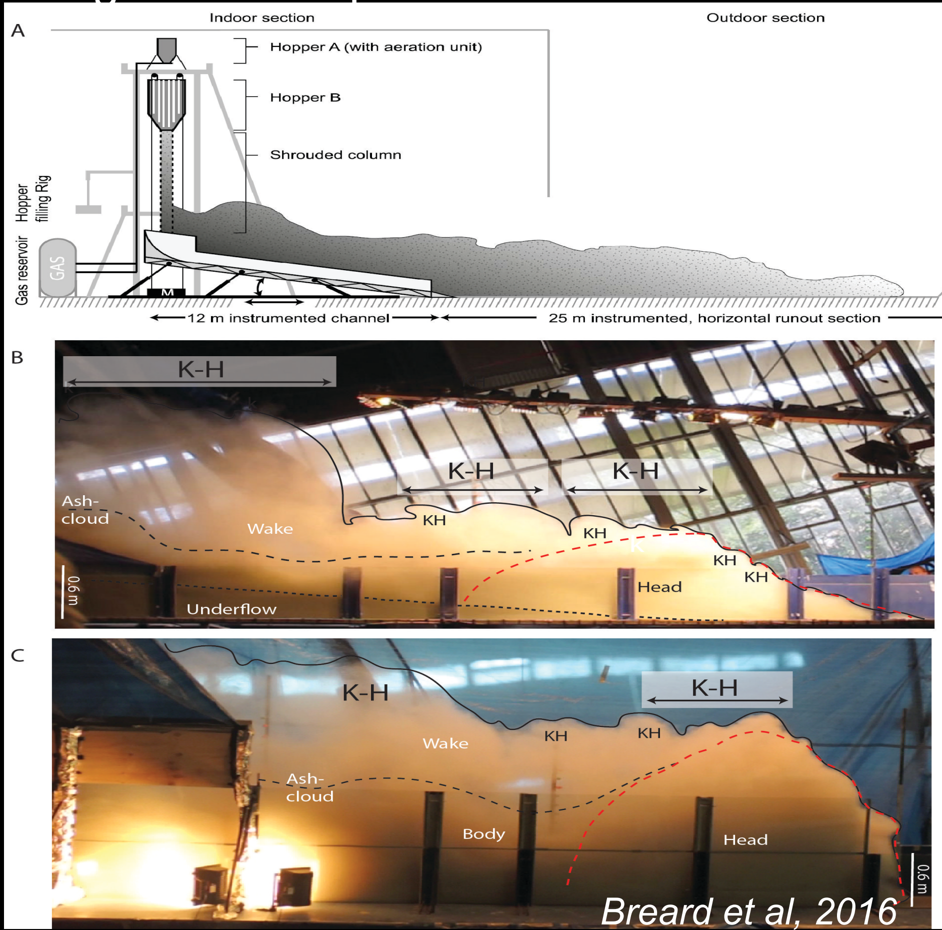

Breard et al, 2016

Smithsonian Facility

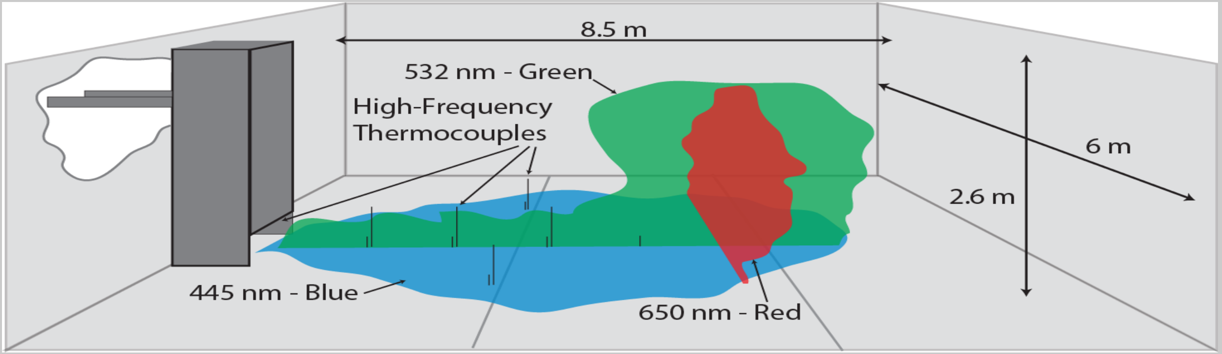

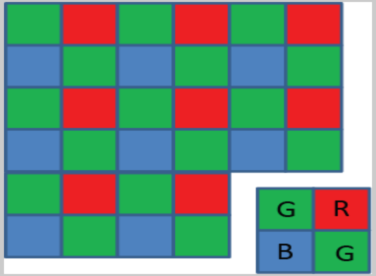

CMOS sensor pixels

- Currents generated by adding (heated) 20 mm talc powder at controlled rated into tank
- Temperature logged with 0.001” K-type thermocouples at 3 Hz
- Currents illuminated with Red, Green, and Blue laser sheets
- Currents recorded with HD video cameras with CMOS sensors – reprojected into dimensional planes
- Rotating laser sheet and high-speed camera for 3D imaging

Disco Laser for 3D Imaging

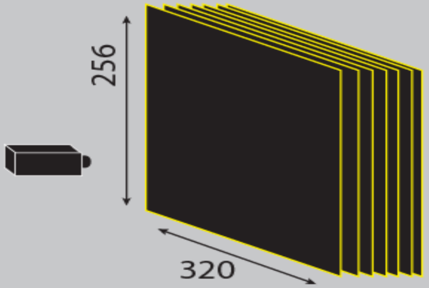

IDT Y3-S1 High Speed Camera
1000 fps at 320x256, 10-bit resolution (binned pixels)
Sequences of 200 images illuminated with "disco laser" collected

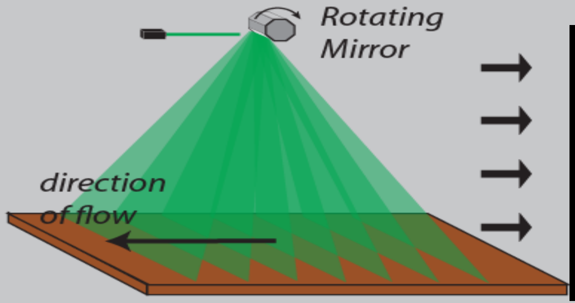

Laser sheet swept at 10 Hz through tank
Sheet generated by four 200-mW green lasers and a rotating 8-sided mirror and

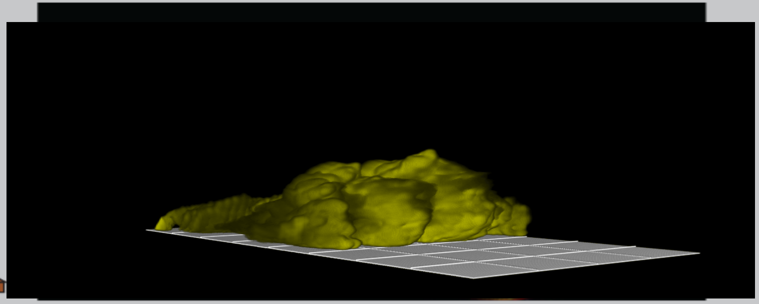

Images corrected for orientation of laser sheet and resampled to 1 cm resolution and "real-world" coordinates
Undistorted image sequences "stacked" for volume reconstructions

Fluidization Experiments

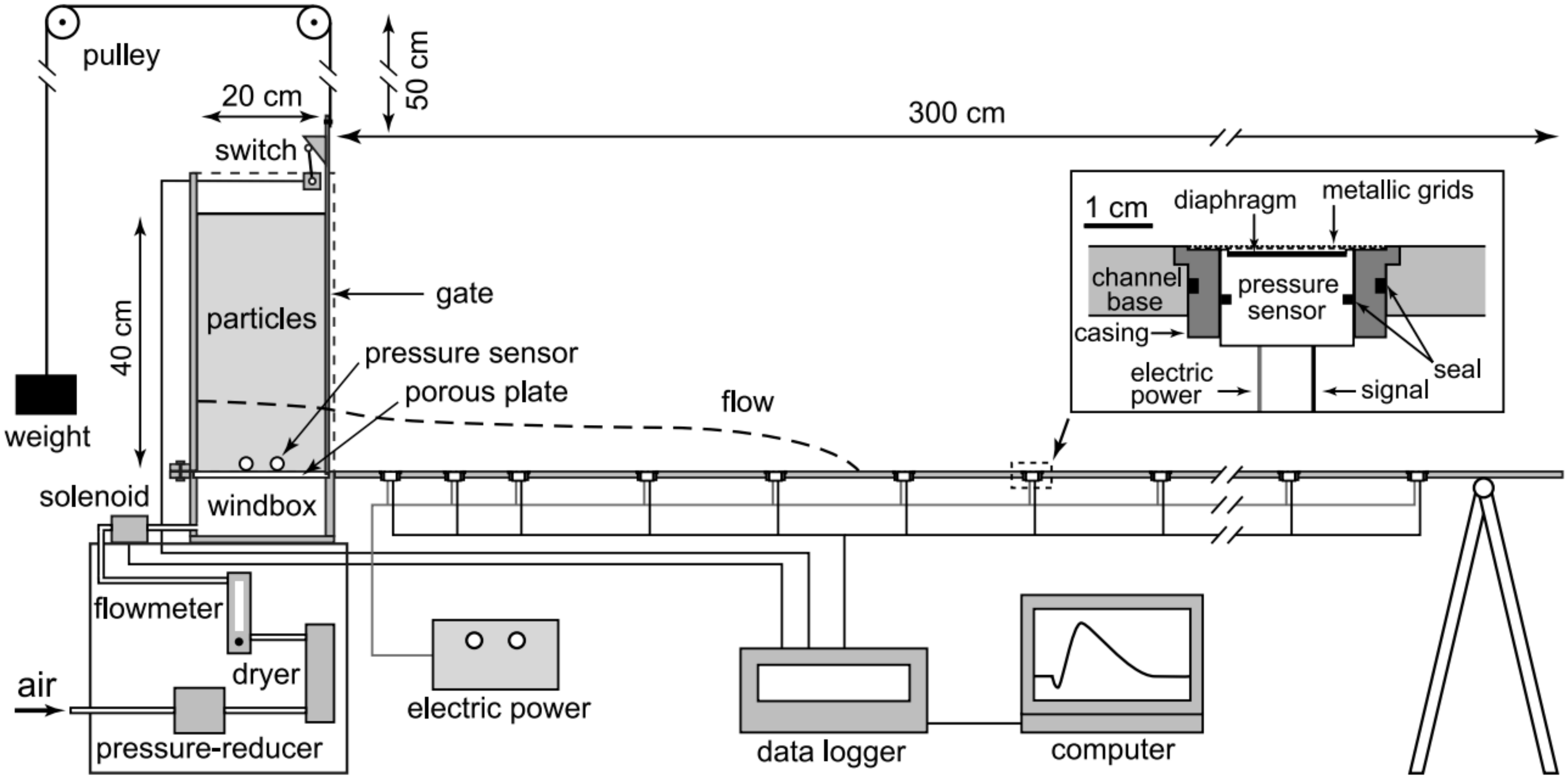

Roche et al. 2010, 2011

Fluidization Experiments

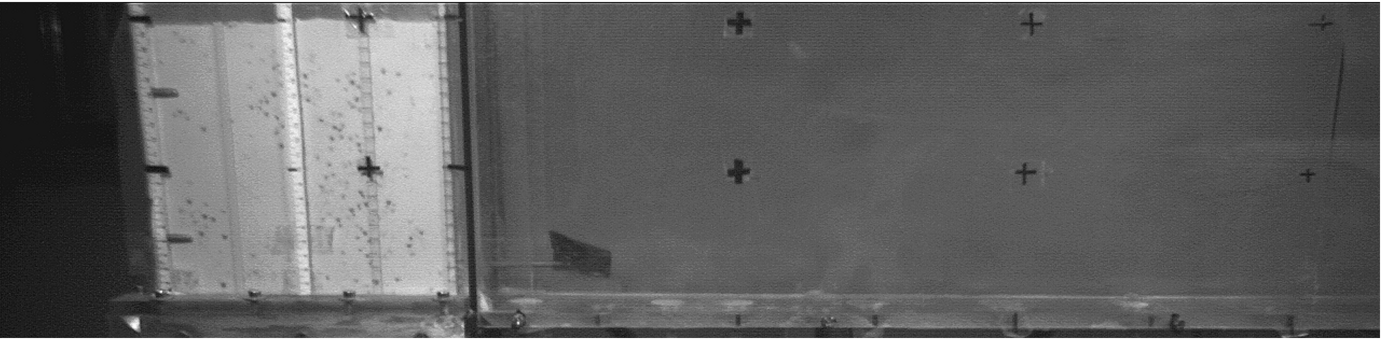

No pore pressure

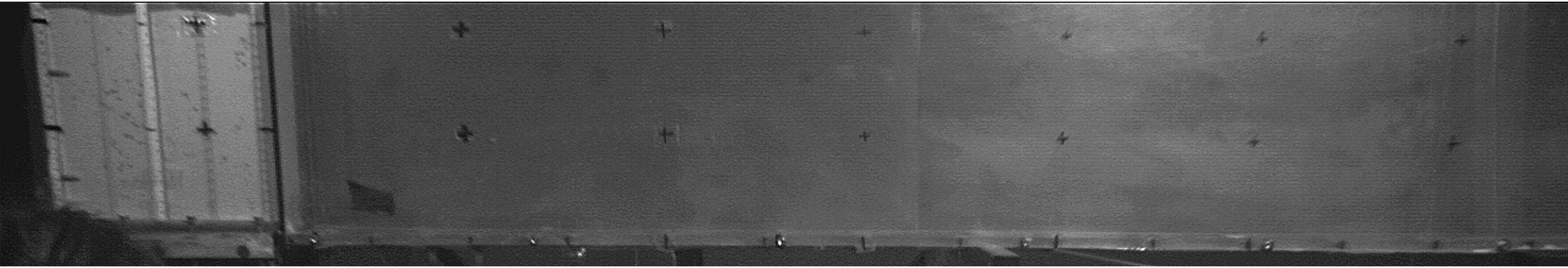

Fluidized

Roche et al. 2010, 2011

PELE Facility

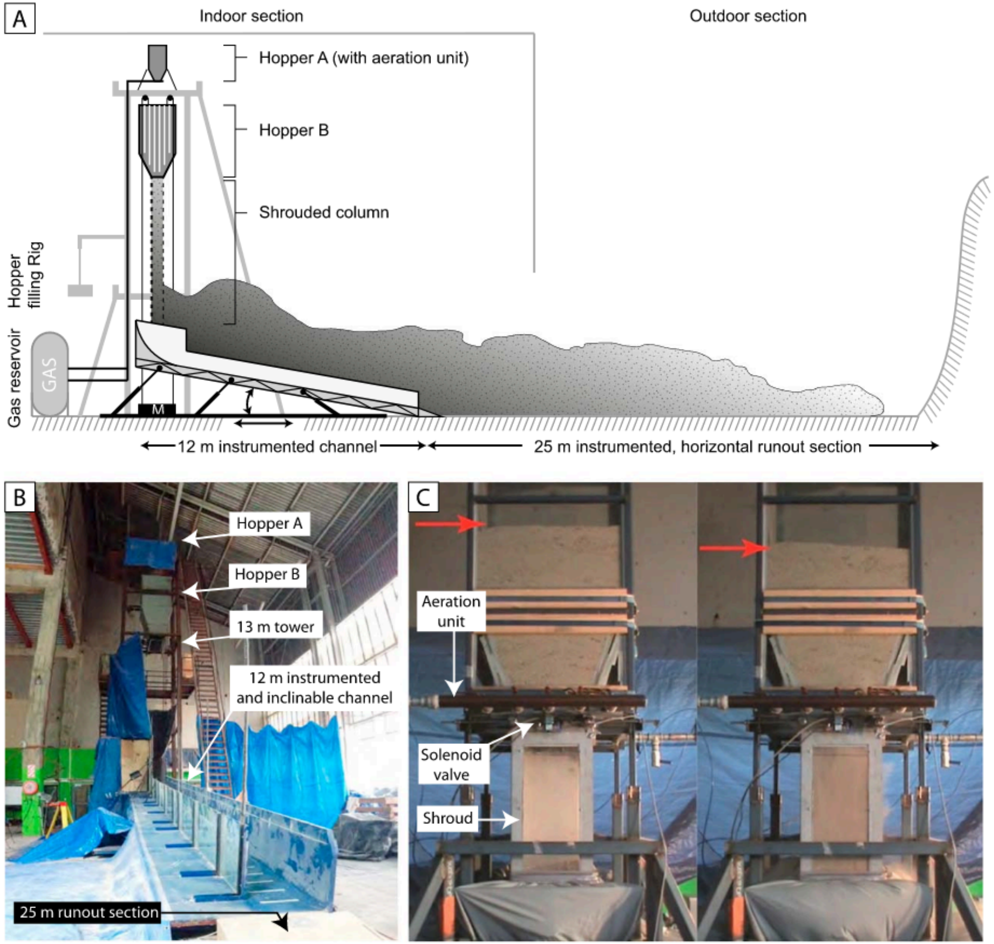

Lube et al., 2015

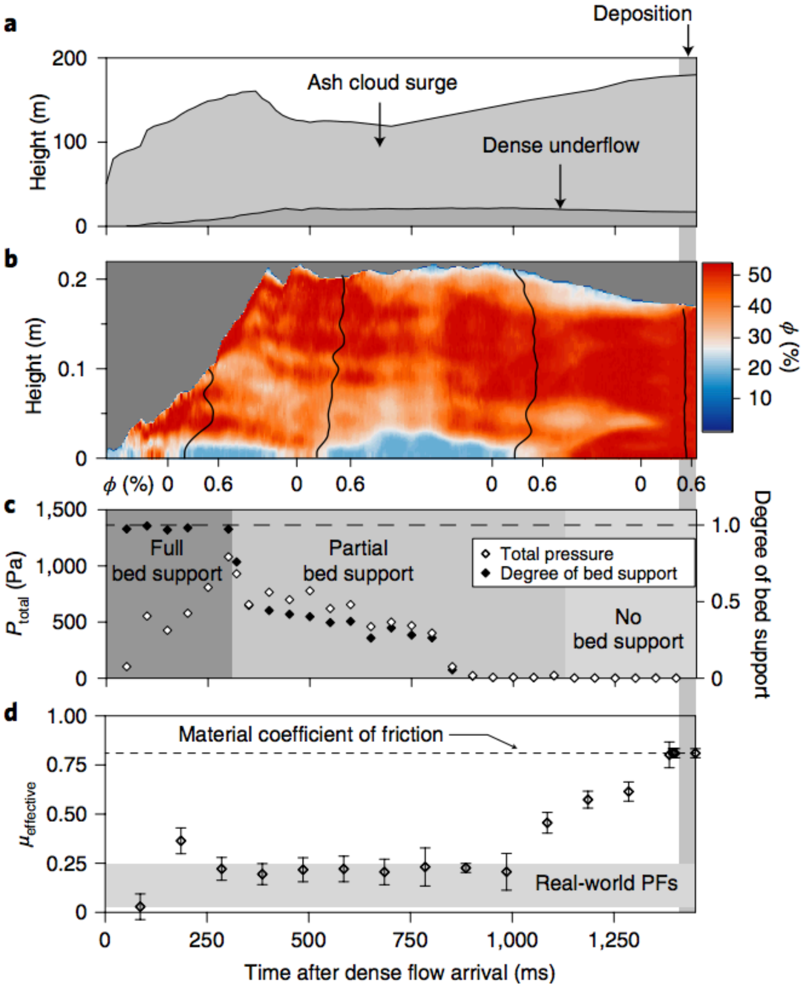

Lube et al., 2019

Modelling PDC

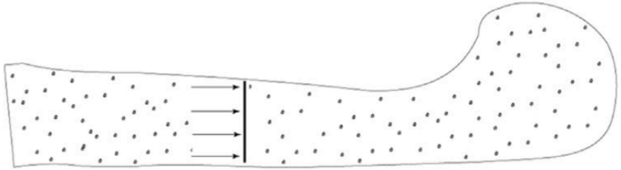

Dilute, 1D models
-Turbulent, homogeneous flows (particles suspended by turbulence)
-Front condition given by constant Froude number

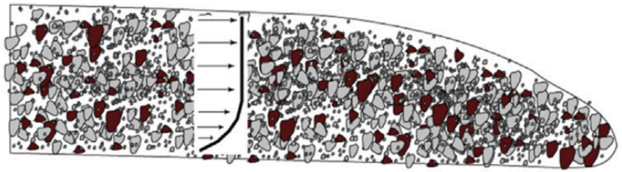

Depth-averaged coulomb models
-Thin, concentrated flows
-Frictional interaction at the bed controls flow motion

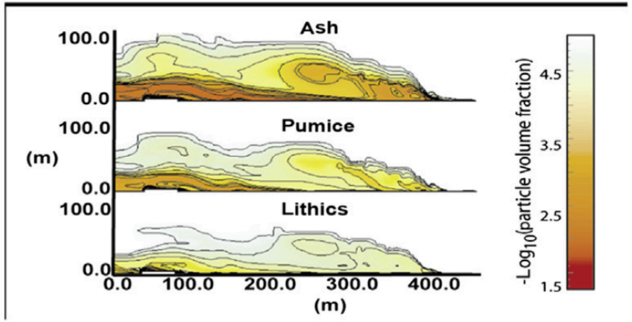

Multiphase models
-Separate conservation equations for multiple particle types
-Drag between the gas and particles transmits momentum between phases

Box models for suspension driven gravity currents

Dade and Huppert, 1994; Dade et al., 1994; Dade and Huppert, 1995a; Dade and Huppert, 1995b, Dade and Huppert, 1996; Dade, 2003.

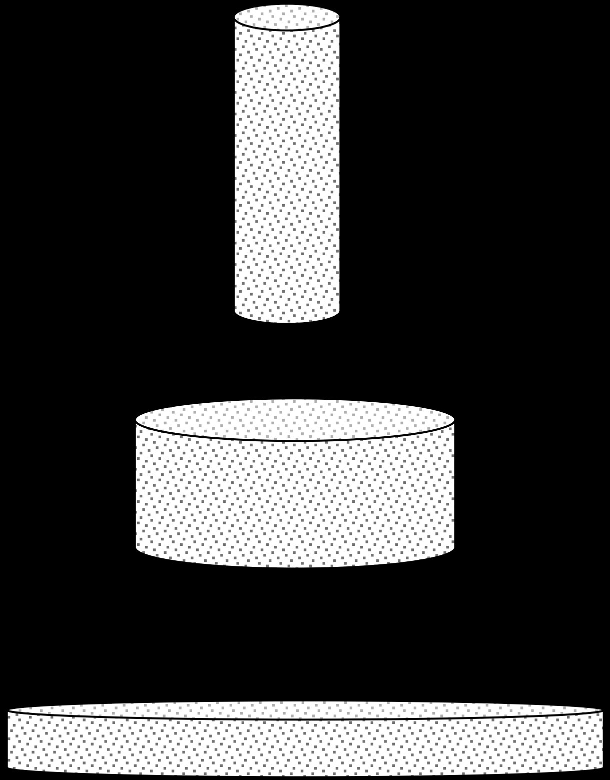

Assumptions:

1. Homogeneous current
2. No particle-particle interaction
3. No entrainment
4. Constant volume
5. Dilution via sedimentation
6. Front condition described by a constant Froude number

Box models for suspension driven gravity currents

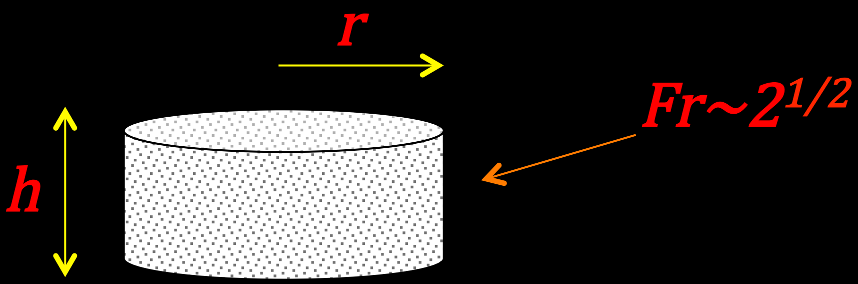

$$u = \frac{dr}{dt} = Fr(hg'\phi)^{\frac{1}{2}}$$

$$V = \Theta \pi r^2 h$$

$$\frac{\partial V\phi}{\partial t} = \frac{-w_s V\phi}{h}$$

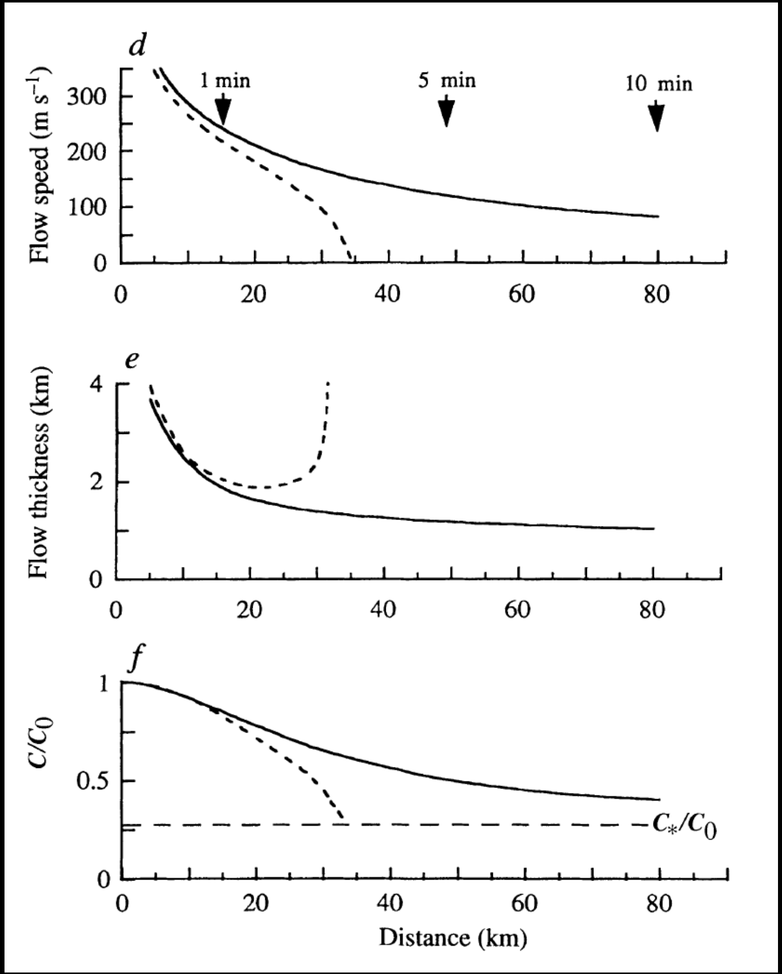

Application to Taupo Ignimbrite

Dade and Huppert, 1996

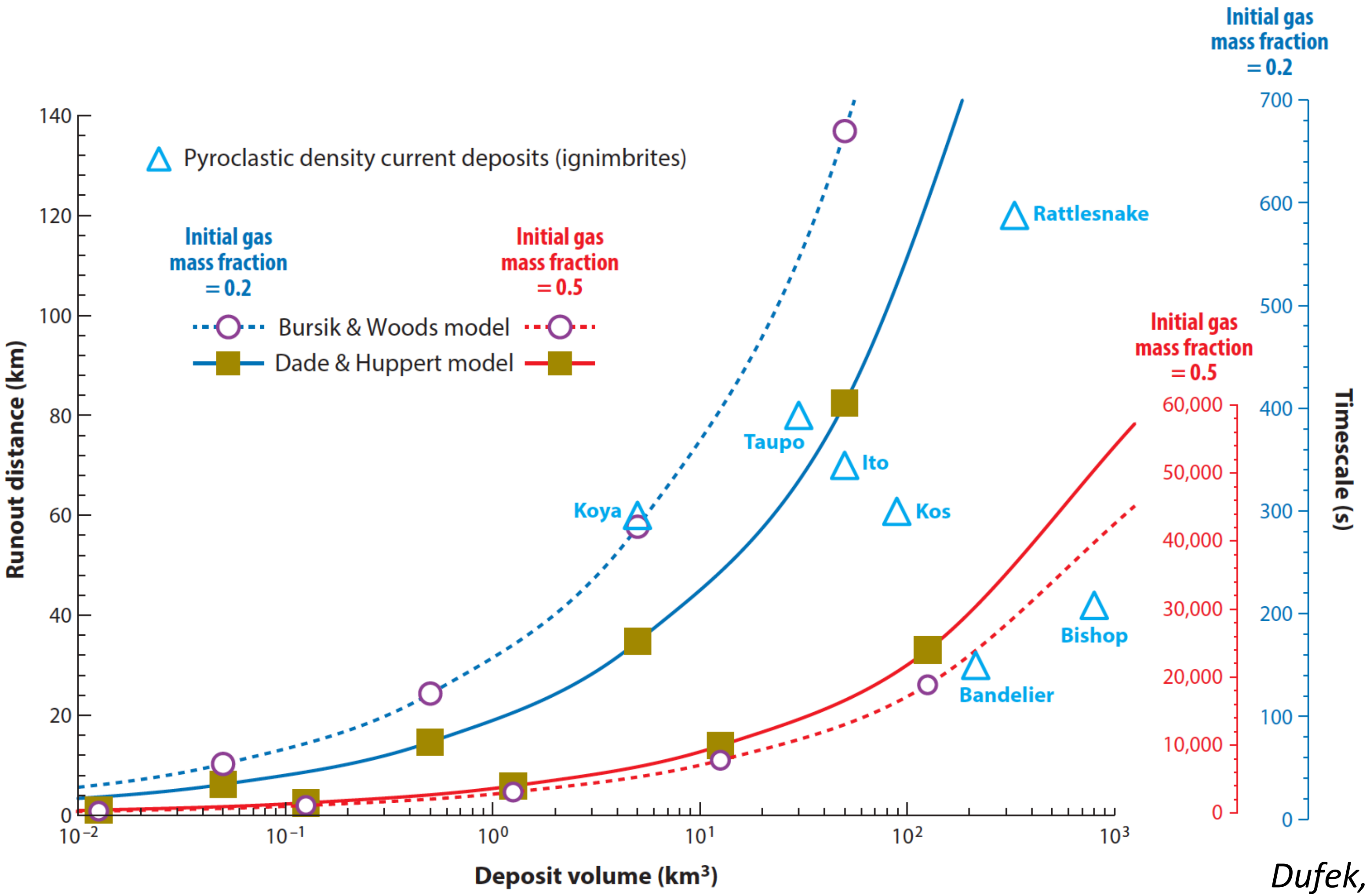

Pyroclastic density current deposits (ignimbrites)
Initial gas mass fraction = 0.2
Initial gas mass fraction = 0.5
Bursik & Woods model
Dade & Huppert model
Rattlesnake
Taupo
Ito
Kos
Koya
Bishop
Bandelier
Initial gas mass fraction = 0.2
Initial gas mass fraction = 0.5
Runout distance (km)
Deposit volume (km³)
Timescale (s)
0
20
40
60
80
100
120
140
10⁻²
10⁻¹
10⁰
10¹
10²
10³
0
10,000
20,000
30,000
40,000
50,000
60,000
0
100
200
300
400
500
600
700

Dufek, 2016

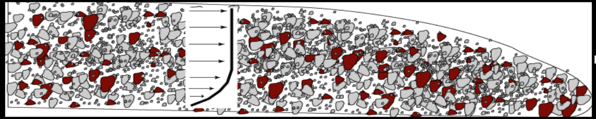

Depth-Averaged Coulomb Models:

- **Titan2D** (Pitman et al., 2000, Sheridan *et al., 2002)*
- ***VolcFlow*** *(Kelfoun and Druitt, 2005)*

Flow Assumptions:

- **Homogenous in space and time (inside current)**
- **Thin, densely packed (Coulomb interaction at base dominates.)**

$$\frac{\partial h}{dt} + \frac{\partial}{\partial x}(hu) + \frac{\partial}{\partial y}(hv) = 0$$

$$\frac{\partial}{\partial t}(hu) + \frac{\partial}{\partial x}(hu^2) + \frac{\partial}{\partial y}(huv) = gh\ \sin\alpha_x - \frac{1}{2}k_{\text{actpass}}\frac{\partial}{\partial x}(gh^2\cos\alpha) + \frac{T_x}{\rho}$$

$$\frac{\partial}{\partial t}(hv) + \frac{\partial}{\partial x}(hvu) + \frac{\partial}{\partial y}(hv^2) = gh\ \sin\alpha_y - \frac{1}{2}k_{\text{actpass}}\frac{\partial}{\partial y}(gh^2\cos\alpha) + \frac{T_y}{\rho}$$

Depth-Averaged Simulations Using different basal interaction

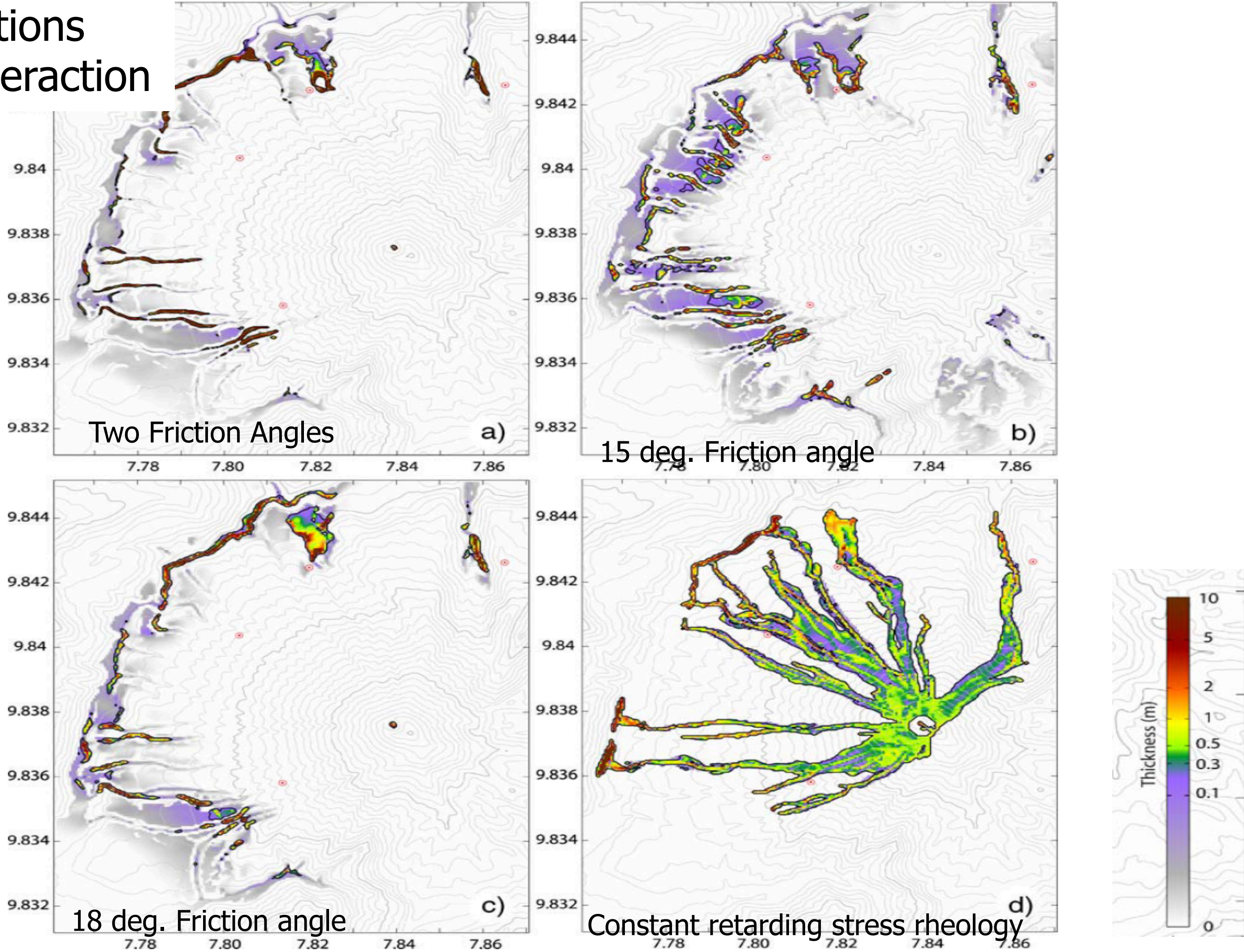

Kelfoun et al, 2009

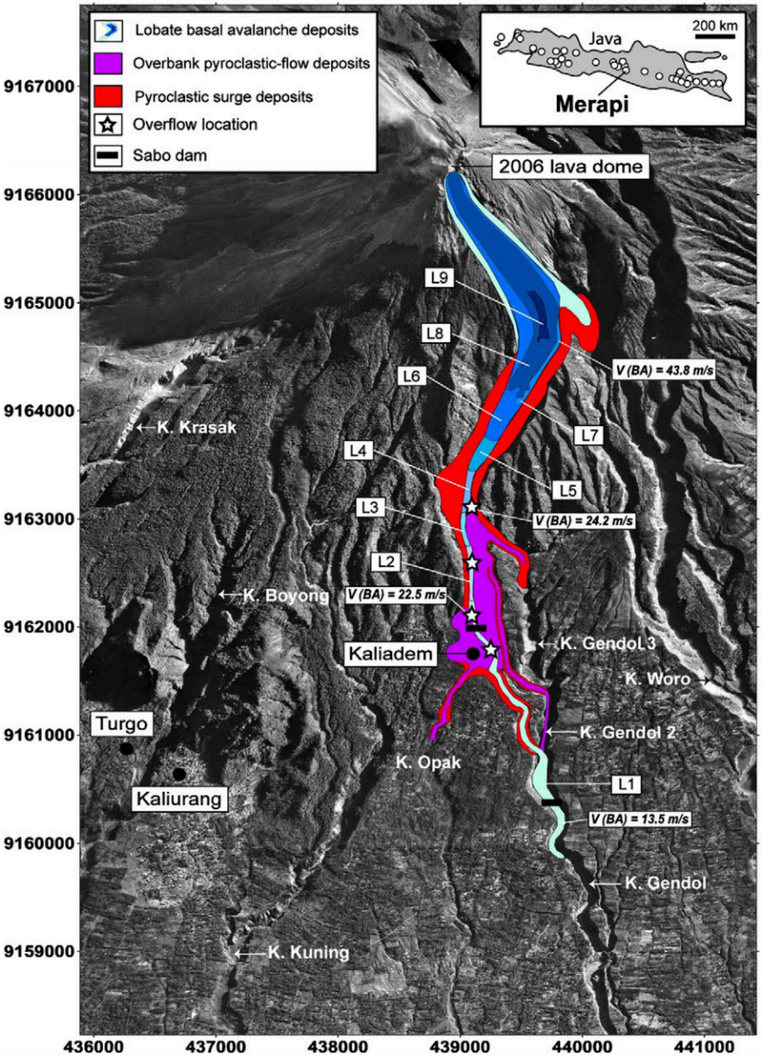

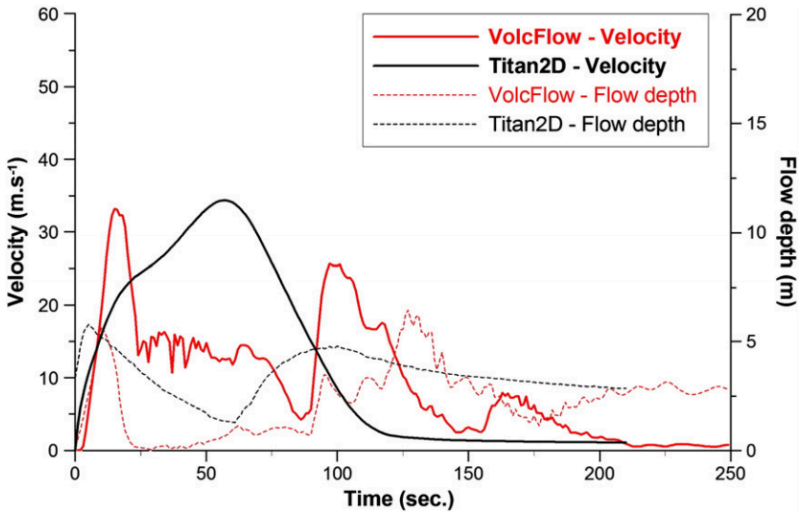

Charbonnier and Gertisser, 2012

Multiphase PDC Simulations

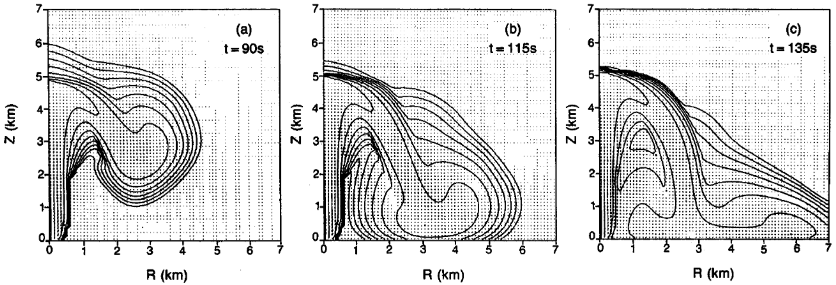

Fig. 8. The log θ_s-$\mathbf{u}_s$ plots of coarse-grained eruption (run 59). Because of poor coupling between the gas and solid phases, structure of the pyroclastic flow is well illustrated by the innermost contour of the lateral flow. A relatively thick head with a slight overhang is shown, followed by a relatively thinner body of the flow.

Valentine and Wohletz (1989)

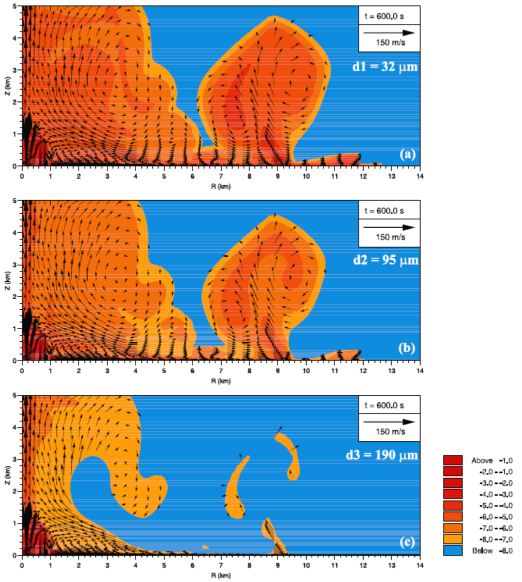

Neri et al (2003)

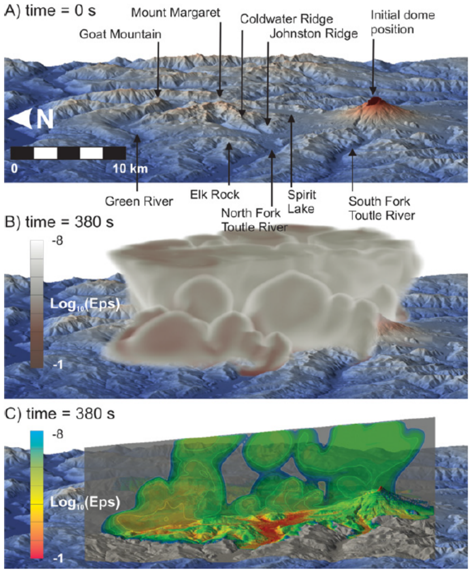

Esposti Ongaro et al. (2011)

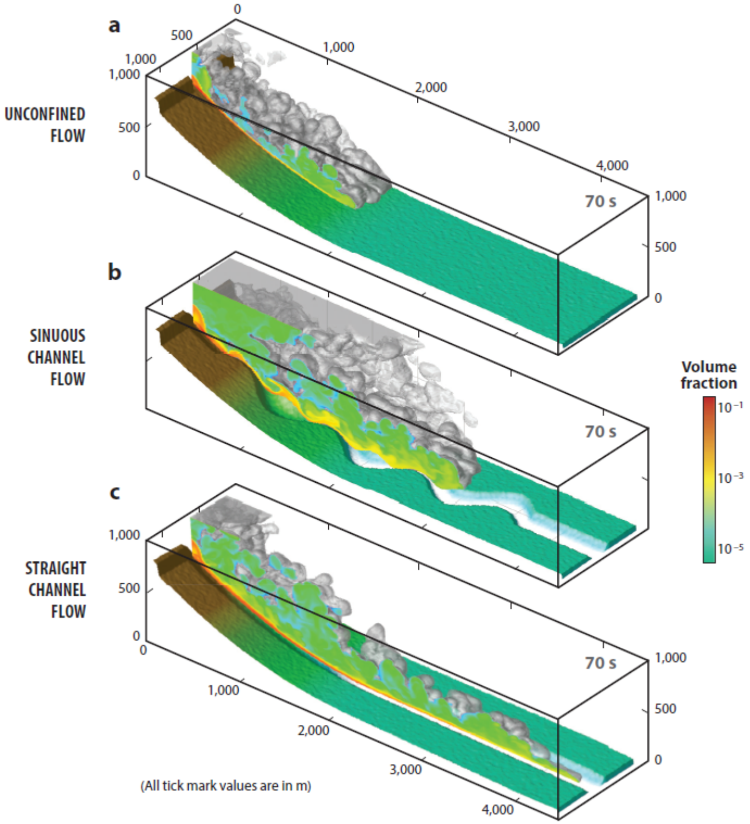

Dufek (2016)

Multi-fluid and Lagrangian Modeling Approach

EEL – Eulerian-Eulerian-Lagrangian

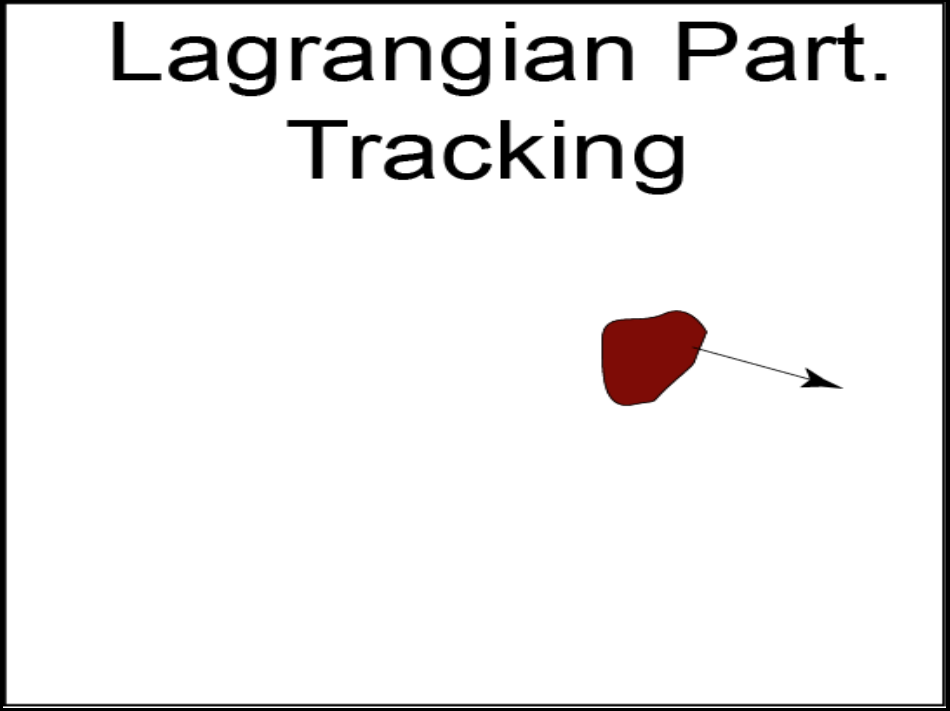

Mean Field Multifluid Equations

Continuity

$$\frac{\partial}{\partial t'}\left({}^{m}\alpha\,{}^{m}\rho'\right)+\frac{\partial}{\partial x'}\left({}^{m}\alpha\,{}^{m}\rho'\,{}^{m}u_i\right)=0$$

Momentum

$$\frac{\partial(\alpha\rho' u'_i)}{\partial t'}+\frac{\partial(\alpha\rho' u'_i u'_j)}{\partial x'_i}=$$

$$\left[\frac{N(\alpha,e)}{{}^{\mathbf{p}}\mathbf{M}_{\mathbf{0}}^{\mathbf{2}}}\right]\frac{\partial(P')}{\partial x'_i}+\left[\frac{1}{\mathbf{Re}}\right]\frac{\partial}{\partial x'_i}\left[\tau_{ij}'\right]+\left[\frac{1}{\mathbf{St}}\right]\left({}^{1}u'_i-{}^{2}u'_i\right)+\left[\frac{1}{\mathbf{Fr_d}^{2}}\right]\alpha\hat{e}_g$$

Thermal Energy

$$\rho' c'_p\left[\frac{\partial T'}{\partial t'}+U_i'\frac{\partial T'}{\partial x_i'}\right]=\left[\frac{1}{\boldsymbol{Pe}}\right]\frac{\partial q'}{\partial x_i'}+\left[\frac{1}{{}^{\boldsymbol{Th}}\boldsymbol{St}}\right]\left(T_p'-T_f'\right)$$

Subscripts:
m=1,2,3 (1 is gas phase and 2 and 3 are particle phases)
s,p=2 and 3 (particle phases)
i,j=1,2 (indices for spatial direction)

[illegible]

Dufek and Bergantz, Journal of Theoretical and Computational Fluid Dynamics, 2007

Lagrangian

$$\frac{\partial v'_{p,i}}{\partial t'} = \frac{1}{St}(u'_i - v'_{p,i}) + \frac{1}{Fr^2}\hat{e}_g$$

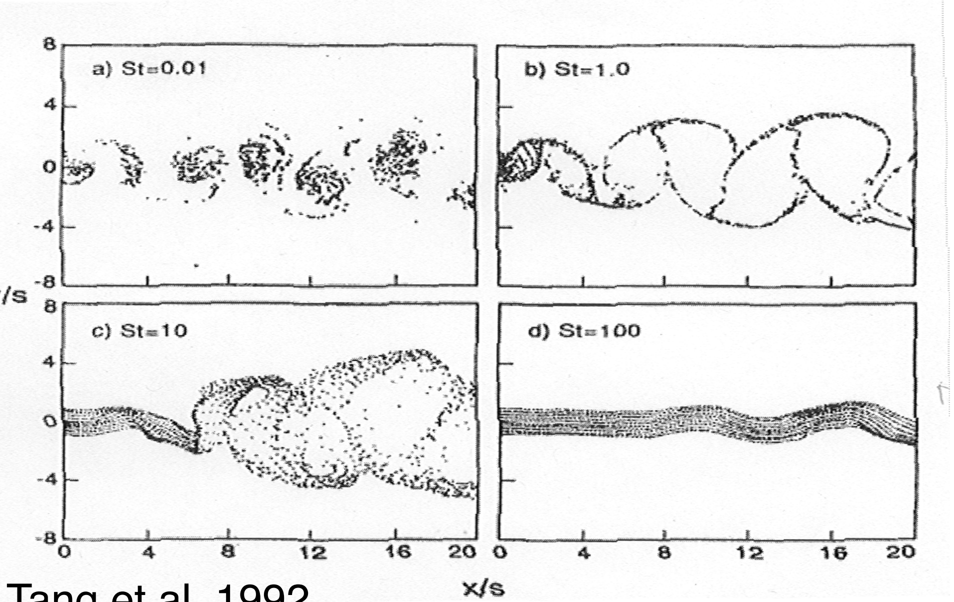

Tang et al. 1992

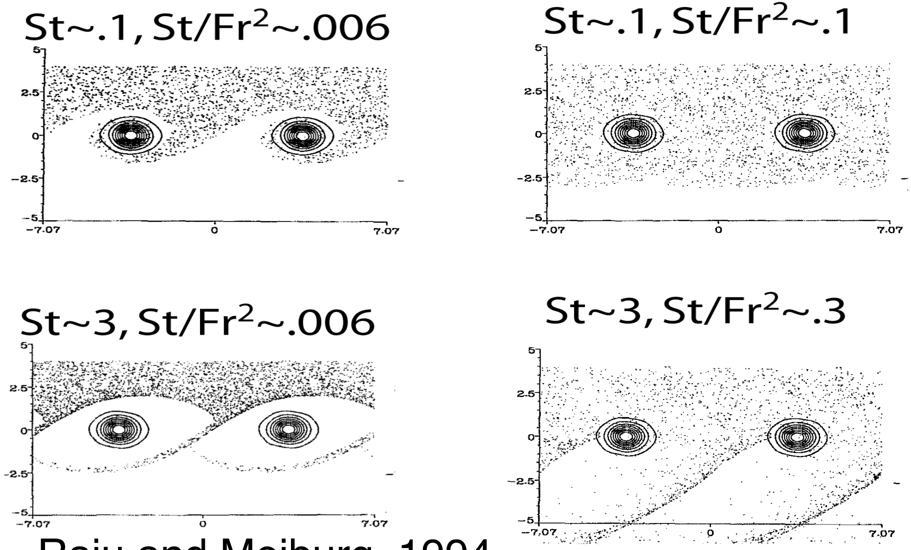

Raju and Meiburg, 1994

Validation

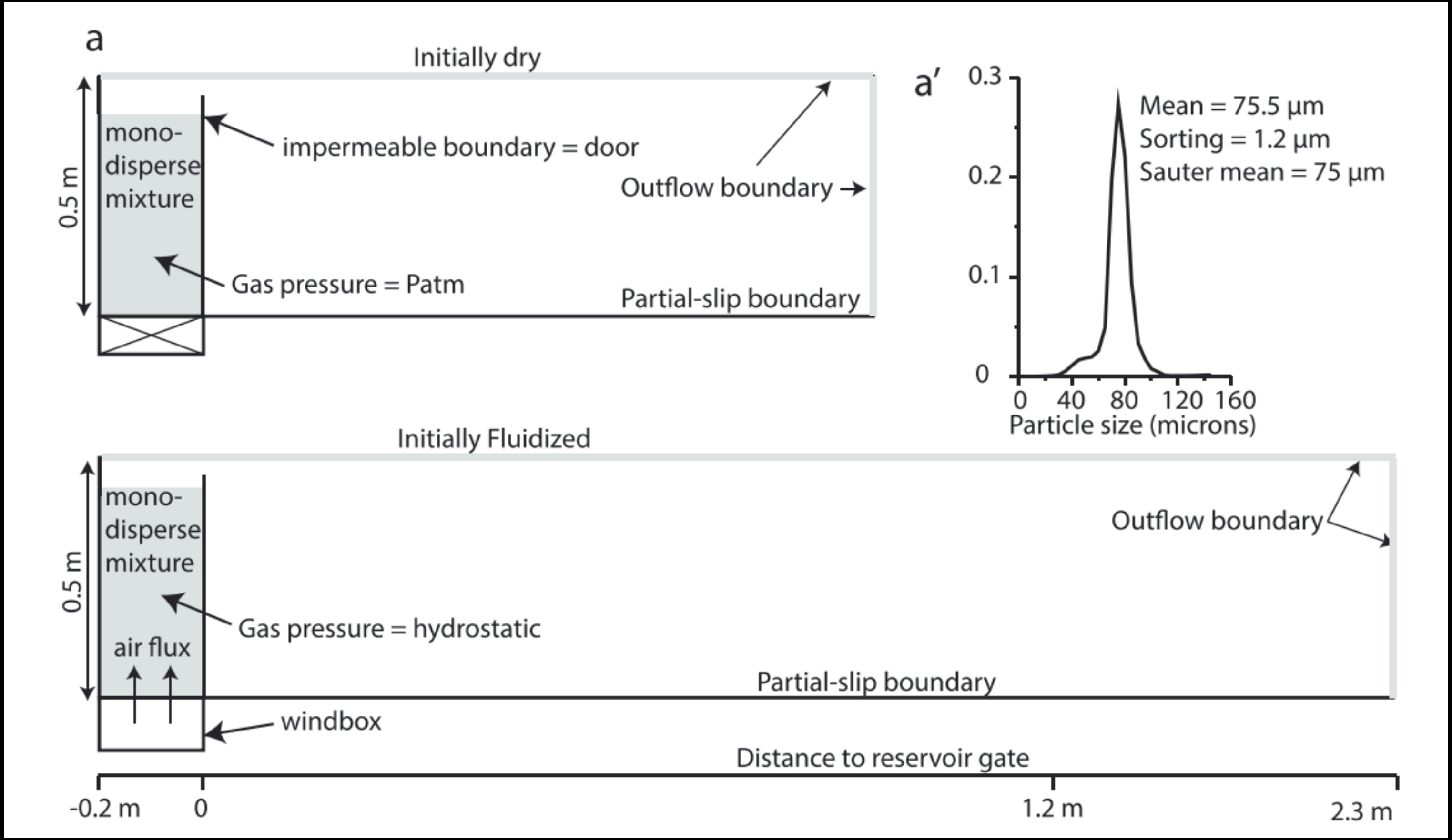

Comparison with Fluidization Experiments of Roche et al., 2010

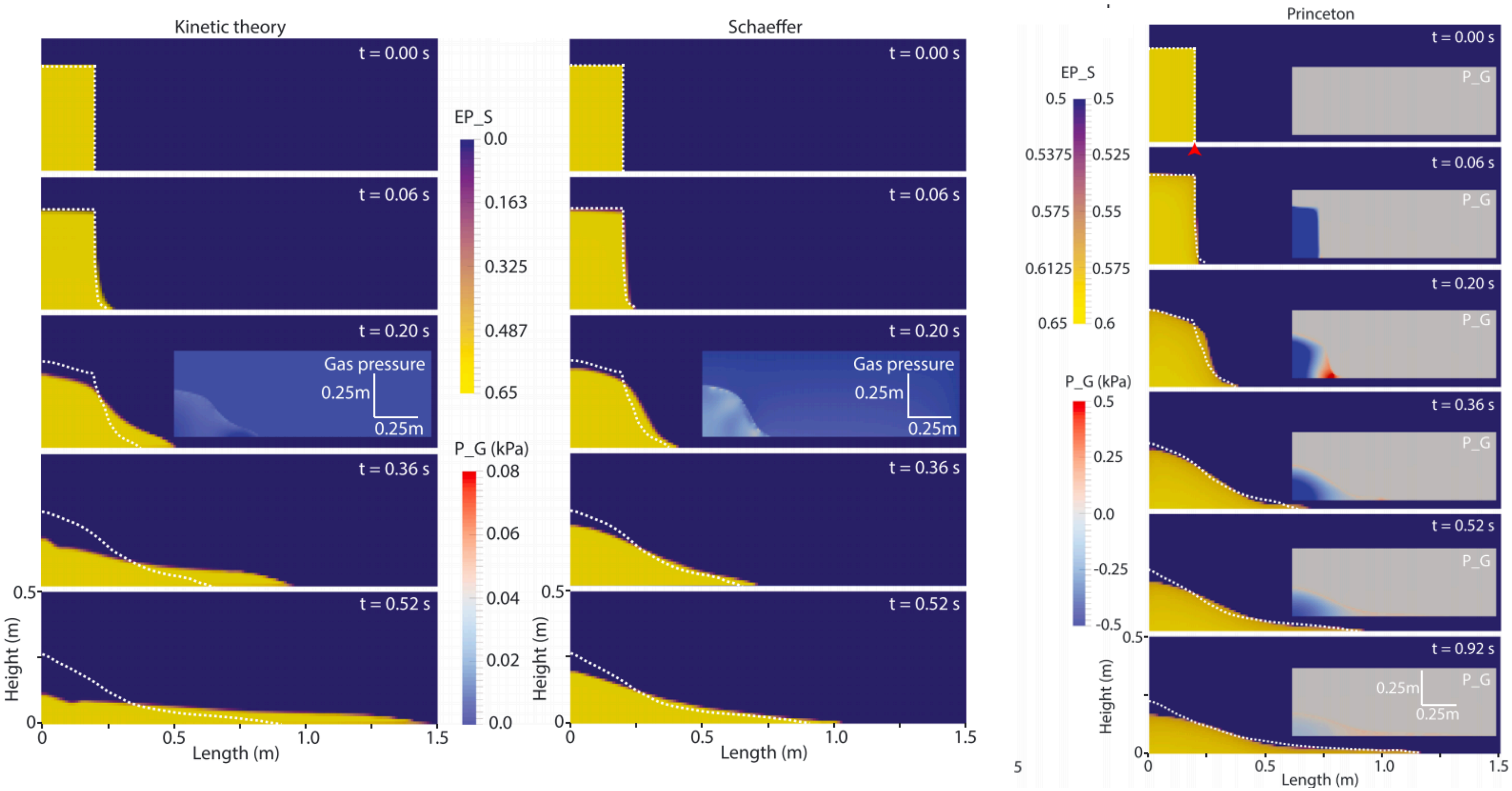

Breard, Dufek and Roche, 2019

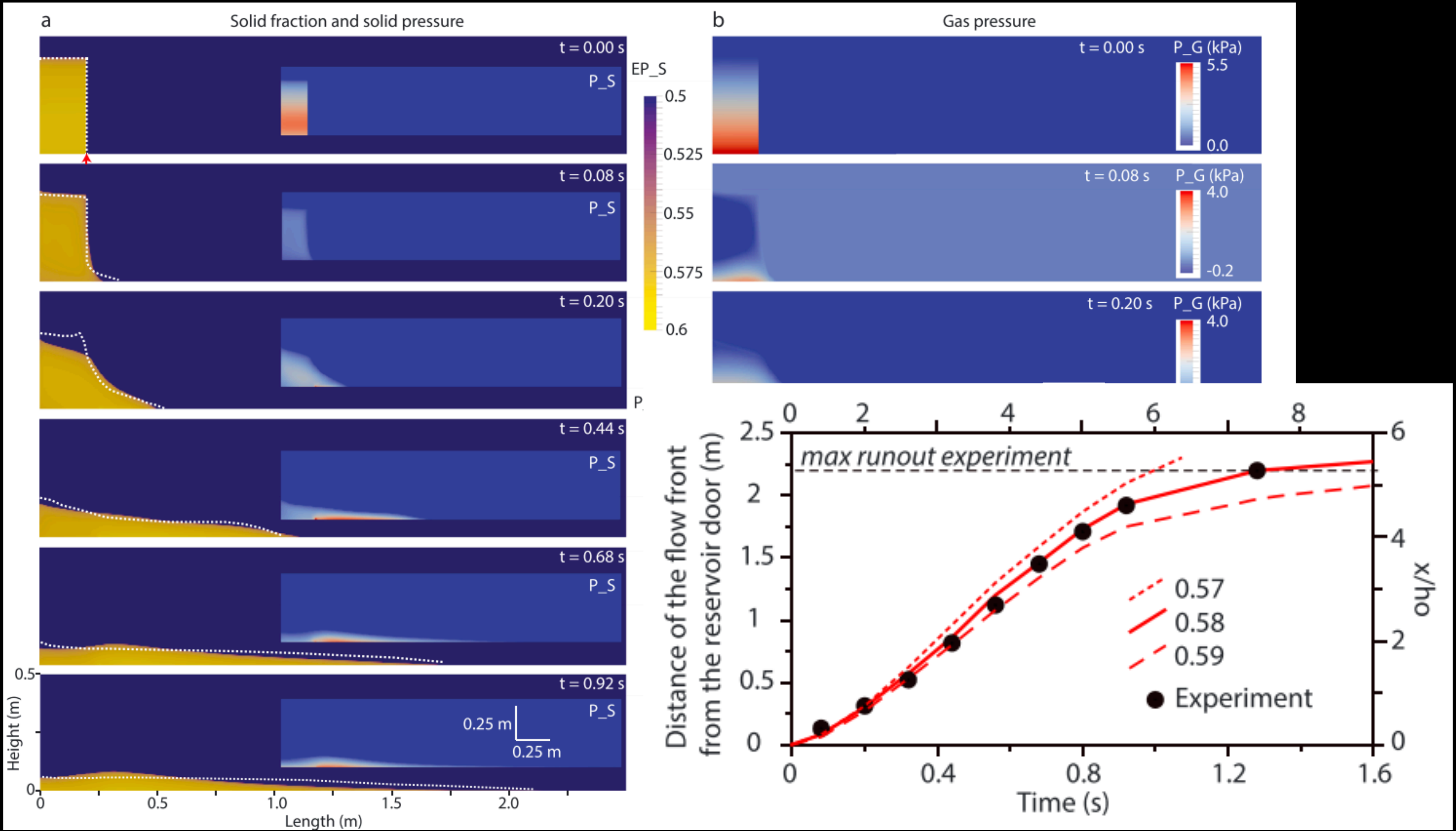

Simulation of fluidized current using frictional model of Srivastava and Sundaresen, 2003

Initial and boundary conditions: inlet conditions

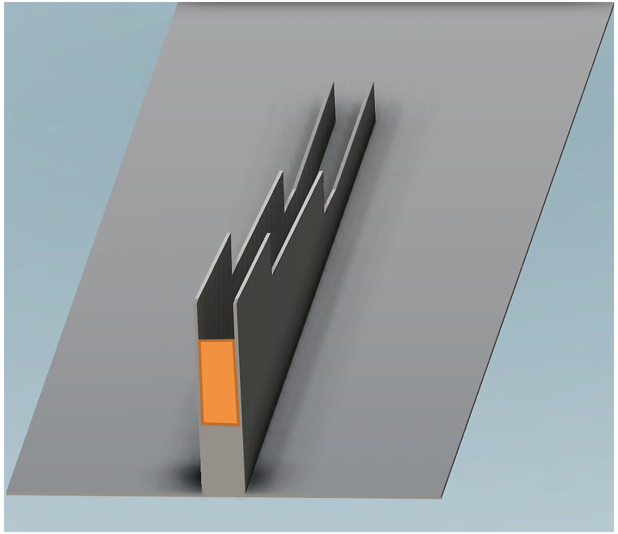

Mass inflow boundary condition are derived from experimental data:

1) Set a vertical velocity profile for the u (parallel to slope) velocity component (decomposed in u, v for the Cartesian MFIX grid)
2) Set a vertical solid concentration profile
3) Set a temperature profile to gas and solid
4) Optional: set a gas pressure at inlet since the code is for compressible flows
5) Set a grain-size distribution -
Used 1 grain size = the Sauter mean diameter of 33 microns.
6) Set a solid density = 2385.93 Kg/m3

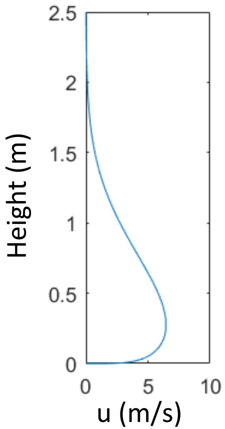

Simulations 1 and 3: steady velocity at inlet

Simulation 2: velocity profile has normally distributed fluctuations with a standard deviation of 0.26.

Results from simulation 3 : turbulent energy spectrums

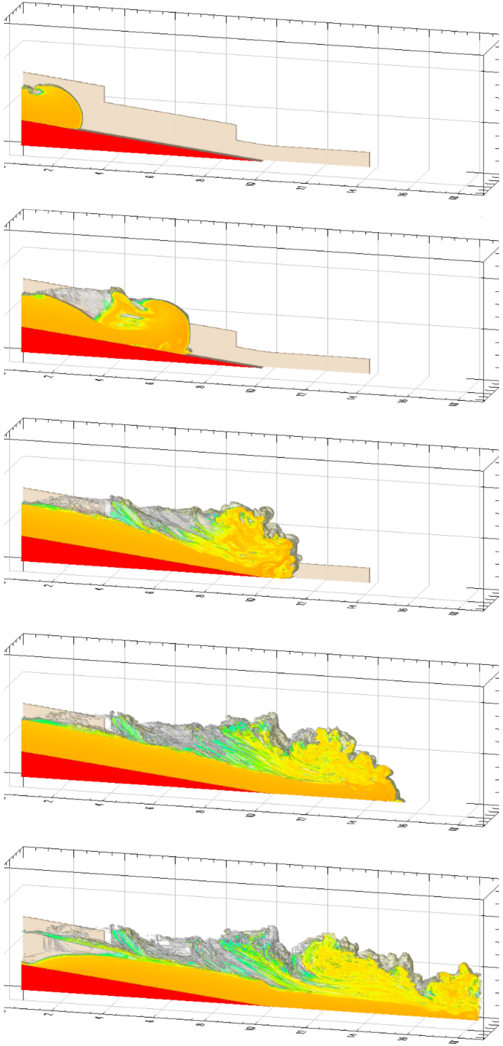

Log (solid concentration)

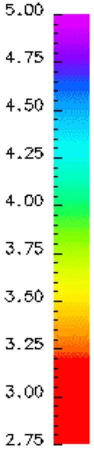

0.3 m above channel

Energy spectrum

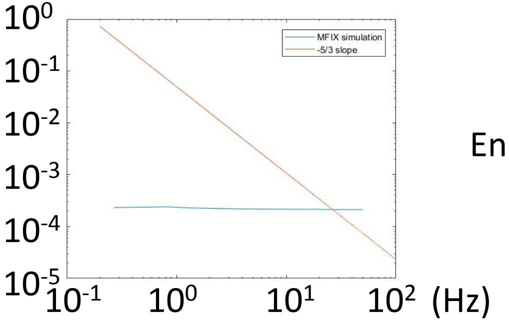

Energy spectrum 0.0125 m from inlet

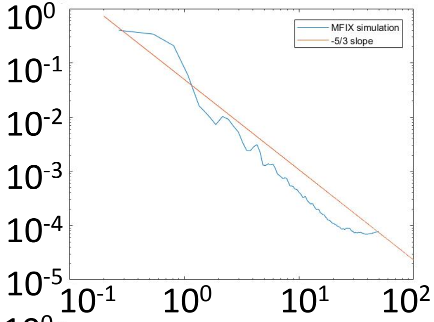

Energy spectrum at 3 m

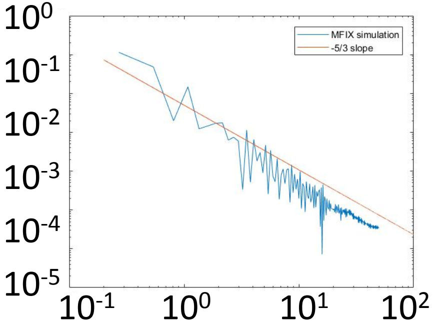

Energy spectrum at 6 m

Flow front kinematics

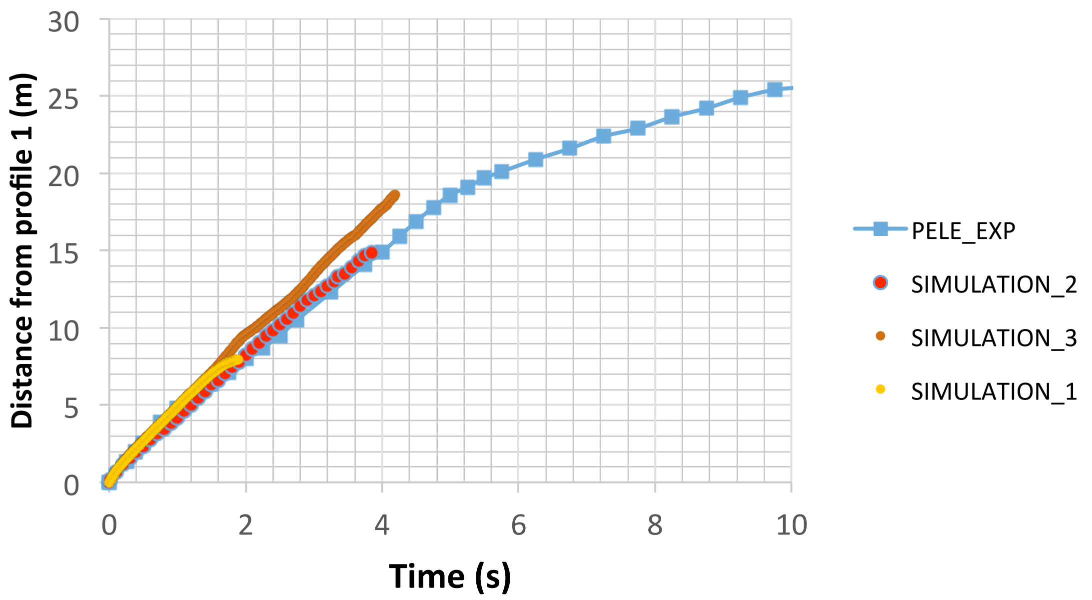

- Change of geometry (wall height) explain the break of slope at ~9m in simulation 3
- Flow front kinematics is better matched if the domain outside the channel is large enough to capture cross-stream ambient air entrainment in the flow

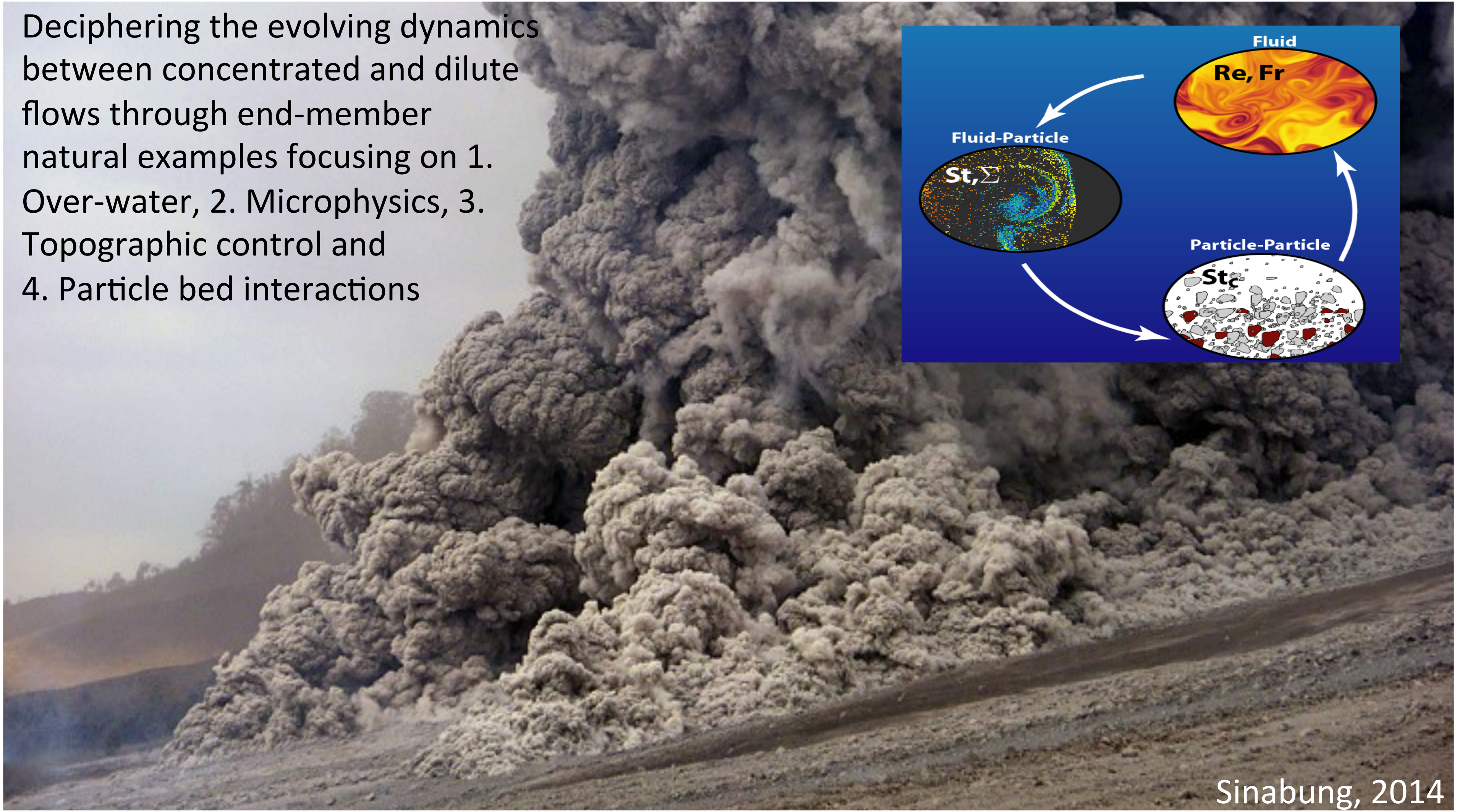
Deciphering the evolving dynamics between concentrated and dilute flows through end-member natural examples focusing on 1. Over-water, 2. Microphysics, 3. Topographic control and 4. Particle bed interactions
Fluid
Re, Fr
Fluid-Particle
St, Σ
Particle-Particle
St_c
Sinabung, 2014

Different Experimental Approaches to Examine the Transport of Multiphase Flows

Microphysical

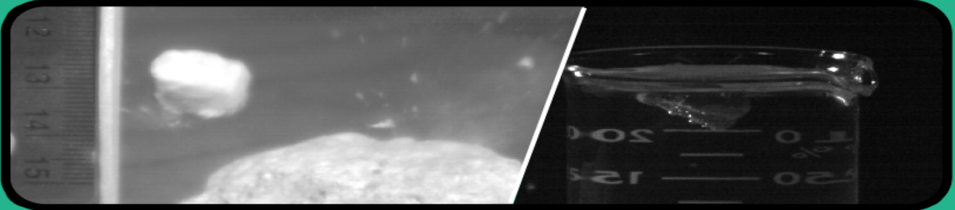

- Emphasis on understanding local particle-particle or particle-fluid interaction
- Useful for developing macroscopic subgrid models

Provides Mass, Momentum, Energy Exchange Rates (R)

Macroscopic

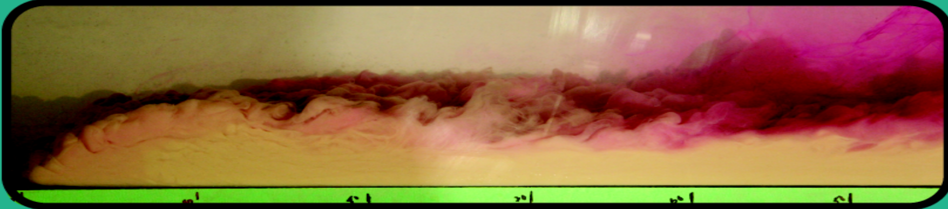

- Emphasis on understanding emergent features and feedback between particle and fluid forcing
- Useful for developing macroscopic subgrid models
- Often have to restrict focus to specific momentum or thermal coupling mechanisms (and not full problem)

Multiphase Equations with Microphysical Processes

Volume fraction of all phases equals 1

$$\sum_k \phi_k = 1$$

Conservation of Mass

$$\frac{\partial}{\partial t}(\phi_k \rho_k) + \frac{\partial}{\partial \mathbf{x_i}}(\phi_k \rho_k \mathbf{u_{k,i}}) = R_k$$

Conservation of Momentum

$$\frac{\partial(\phi_k \rho_k \mathbf{u_{k,i}})}{\partial t} + \frac{\partial(\phi_k \rho_k \mathbf{u_{k,i}} \mathbf{u_{k,j}})}{\partial \mathbf{x_i}} =$$

$$-\phi_k \frac{\partial P}{\partial \mathbf{x_i}} \delta_{ij} + \frac{\partial}{\partial \mathbf{x_i}}\left[\tau_{\mathbf{ij}}\right] + \mathbf{D}_i + \rho_k \phi_k \boldsymbol{g}_2 \delta_{\mathbf{i2}} + R_k \mathbf{u_{k,i}}$$

Mass Exchange

Leaky Boundary Flow

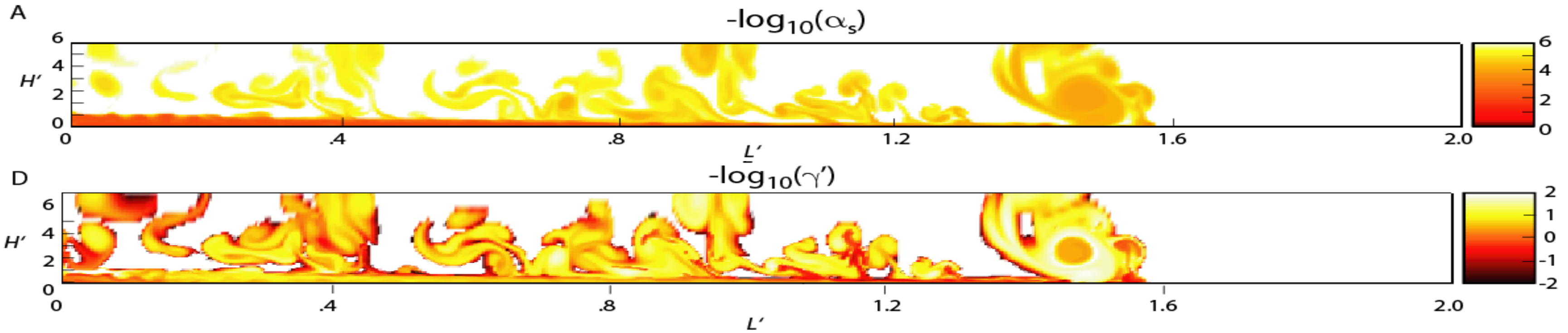

Saltation Boundary Flow

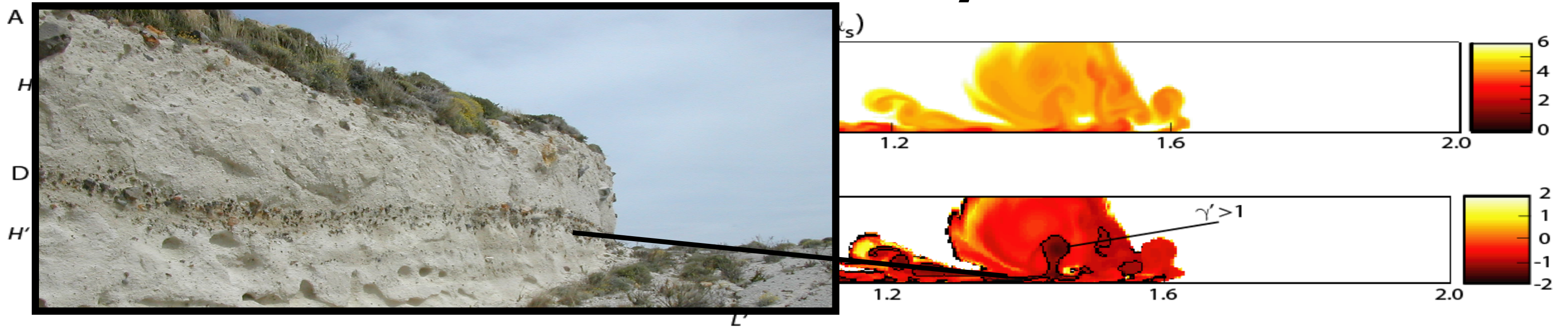

$$\gamma' = \frac{\alpha_2}{\alpha_1} \Big/ \frac{\alpha_2^0}{\alpha_1^0}$$

Dufek and Bergantz, 2007

Runout Distance

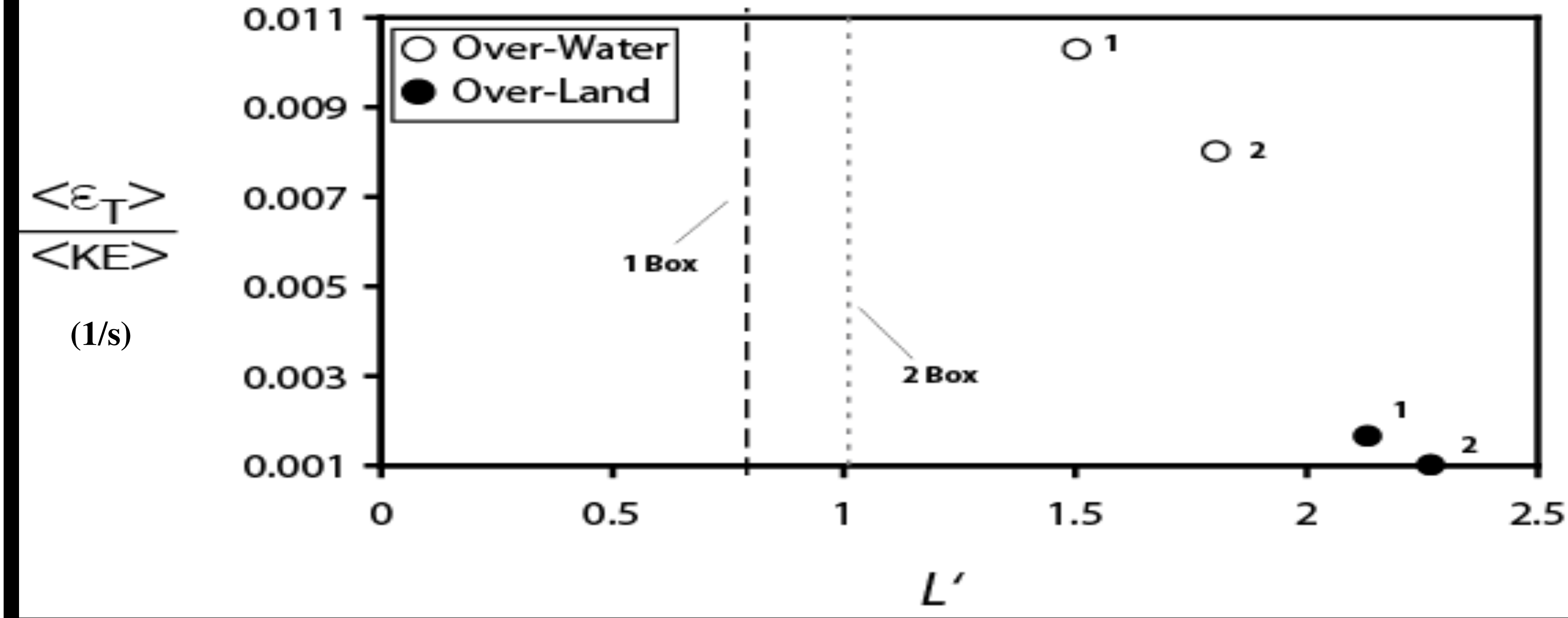

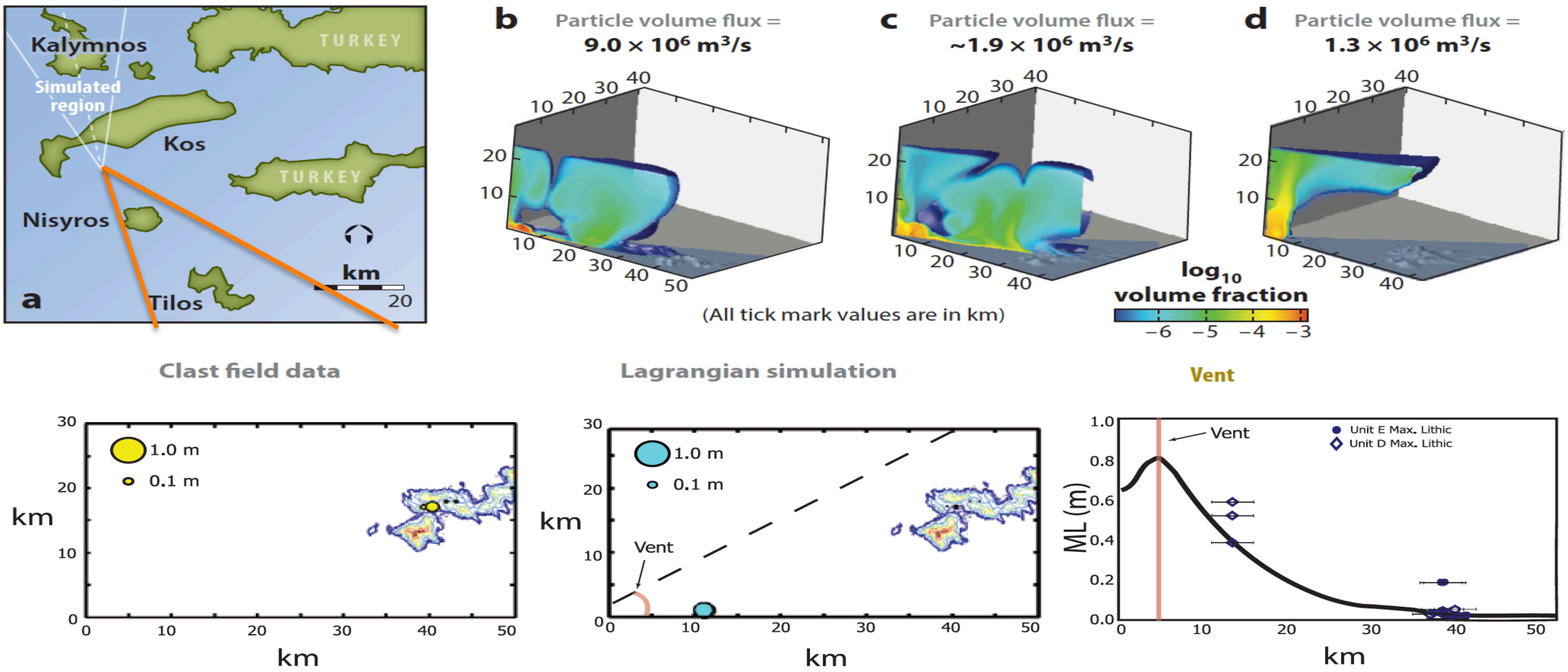

Kalymnos
Simulated region
Kos
TURKEY
TURKEY
Nisyros
Tilos
km
20
a
b
Particle volume flux =
9.0 × 10⁶ m³/s
c
Particle volume flux =
~1.9 × 10⁶ m³/s
d
Particle volume flux =
1.3 × 10⁶ m³/s
log10 volume fraction
−6 −5 −4 −3
(All tick mark values are in km)
Clast field data
1.0 m
0.1 m
km
Lagrangian simulation
1.0 m
0.1 m
Vent
km
Vent
Vent
Unit E Max. Lithic
Unit D Max. Lithic
ML (m)
km

Dufek, 2016

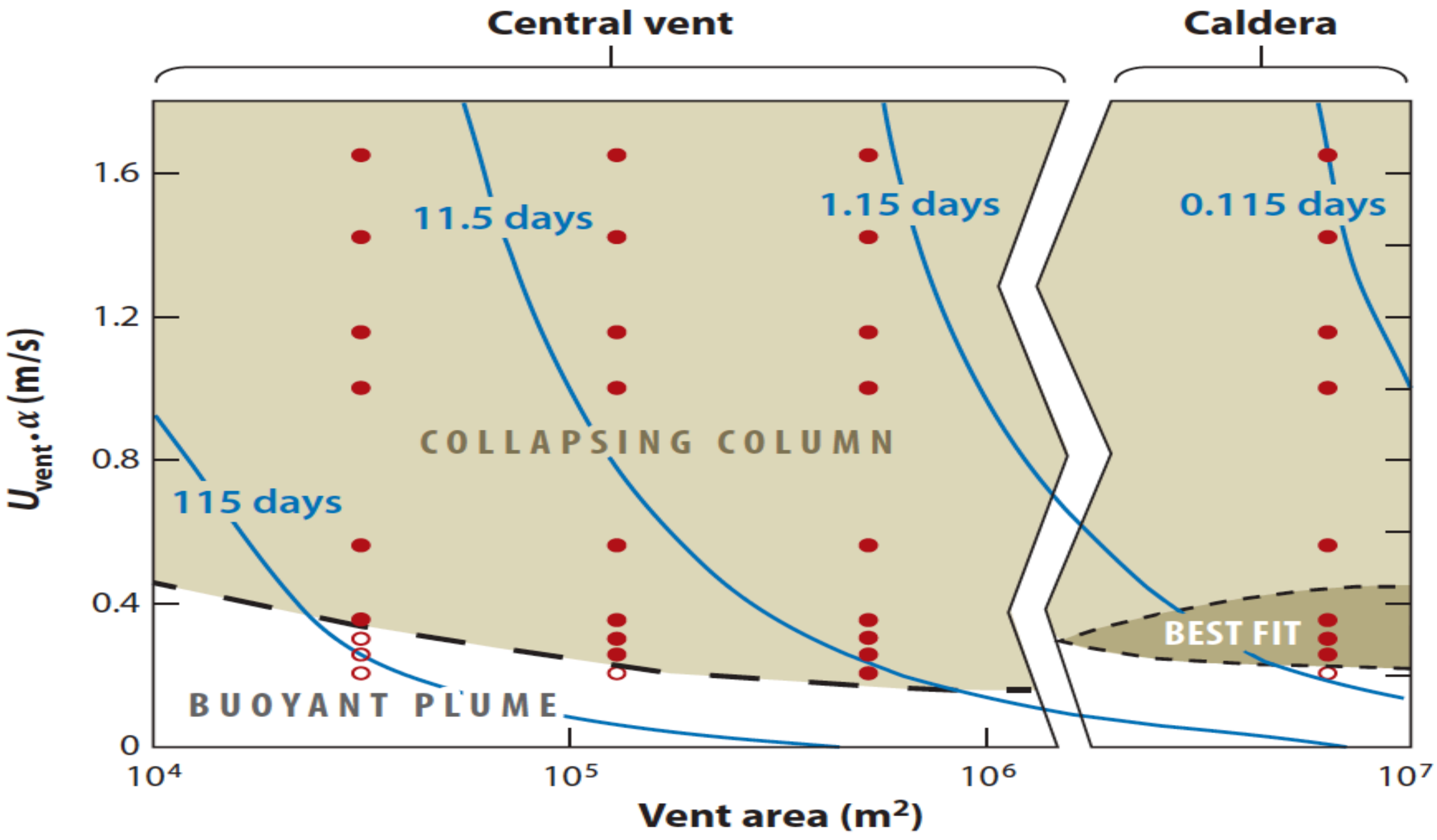

Central vent
Caldera
11.5 days
1.15 days
0.115 days
115 days
COLLAPSING COLUMN
BUOYANT PLUME
BEST FIT
1.6
1.2
0.8
0.4
0
$U_{vent} \cdot \alpha$ (m/s)
10^4
10^5
10^6
10^7
Vent area (m^2)

Comminution in pyroclastic density currents

Mount Saint Helens, USGS

Comminution Mechanisms

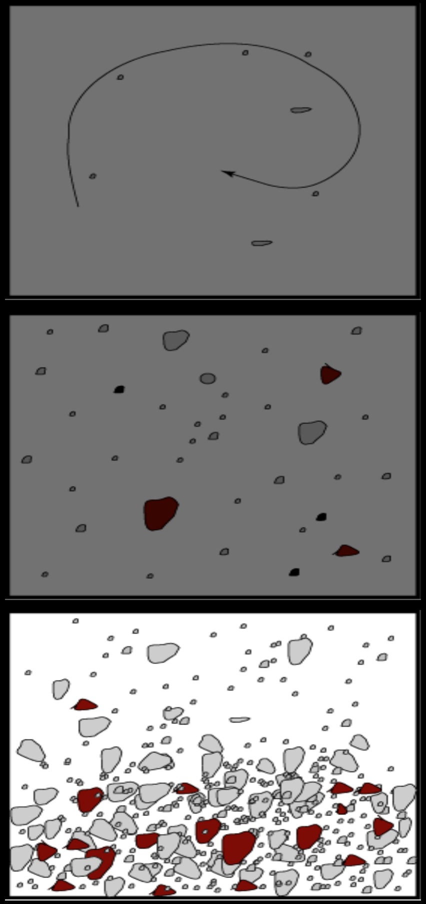

Prolonged Frictional Contact

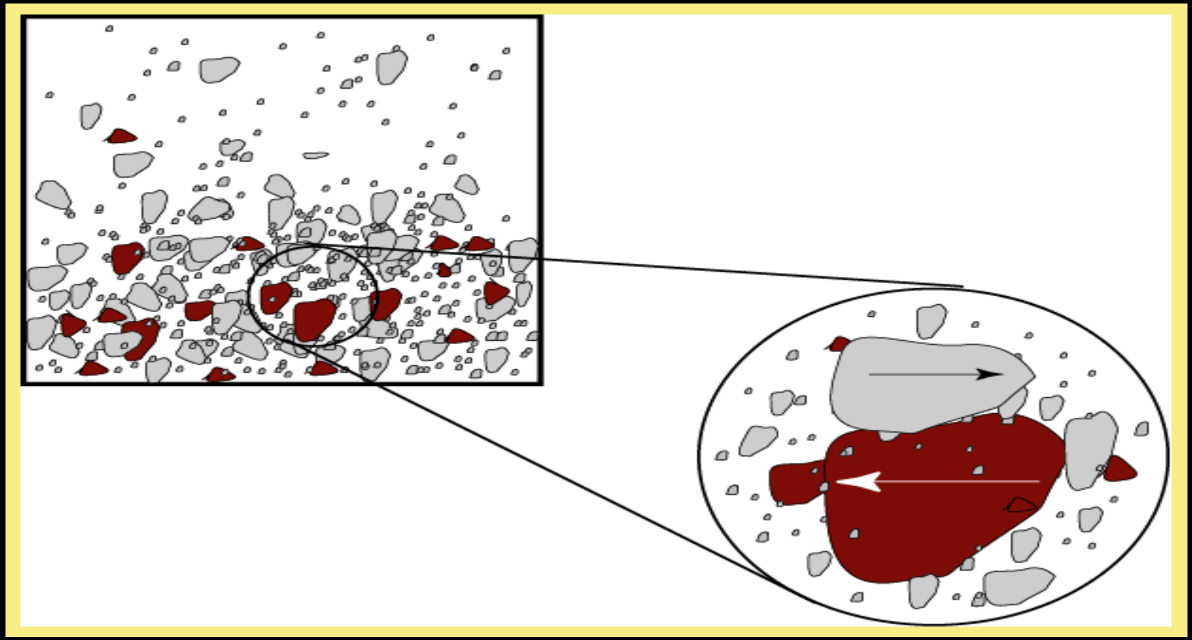

Frictional ash

Comminution Mechanisms

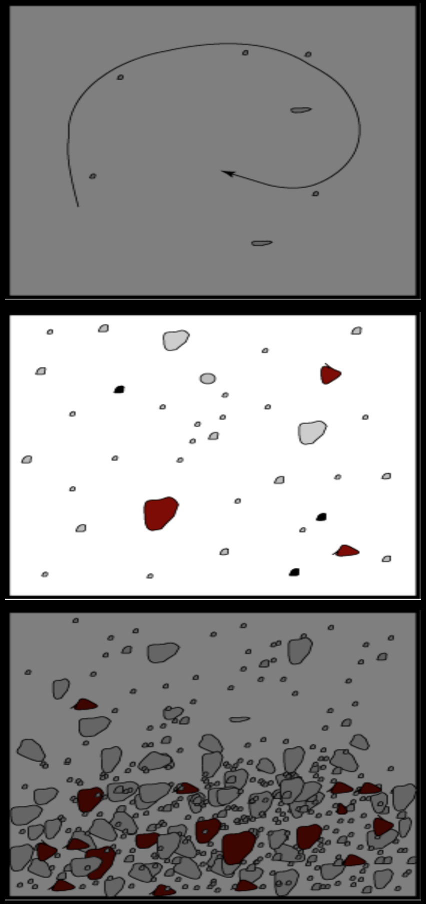

Instantaneous Collisions

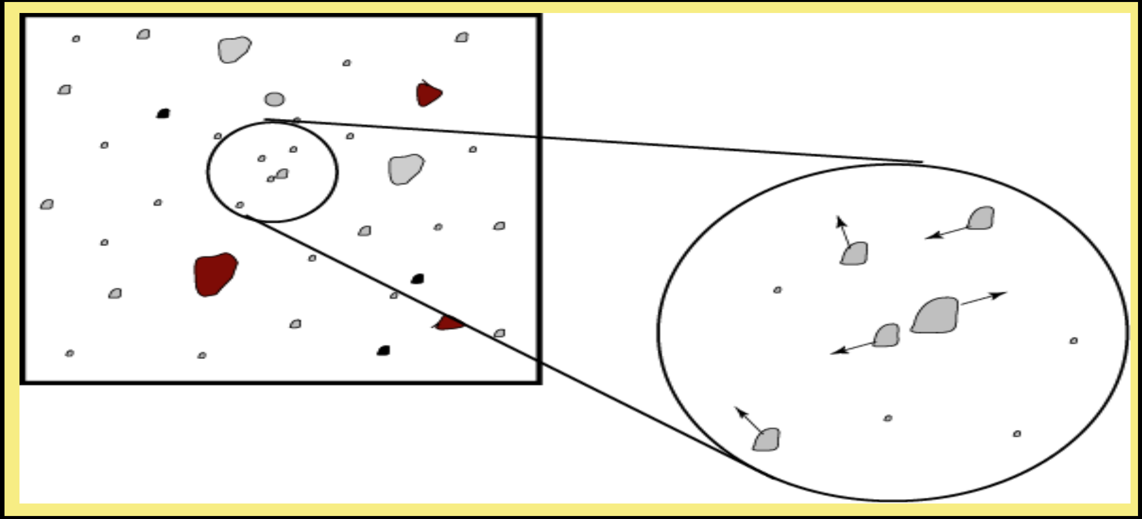

Collisional ash

Ash characteristics

- Only ash is made at small collisional velocity (< 30 m/s) -- not a power law or fractal distribution of sizes)

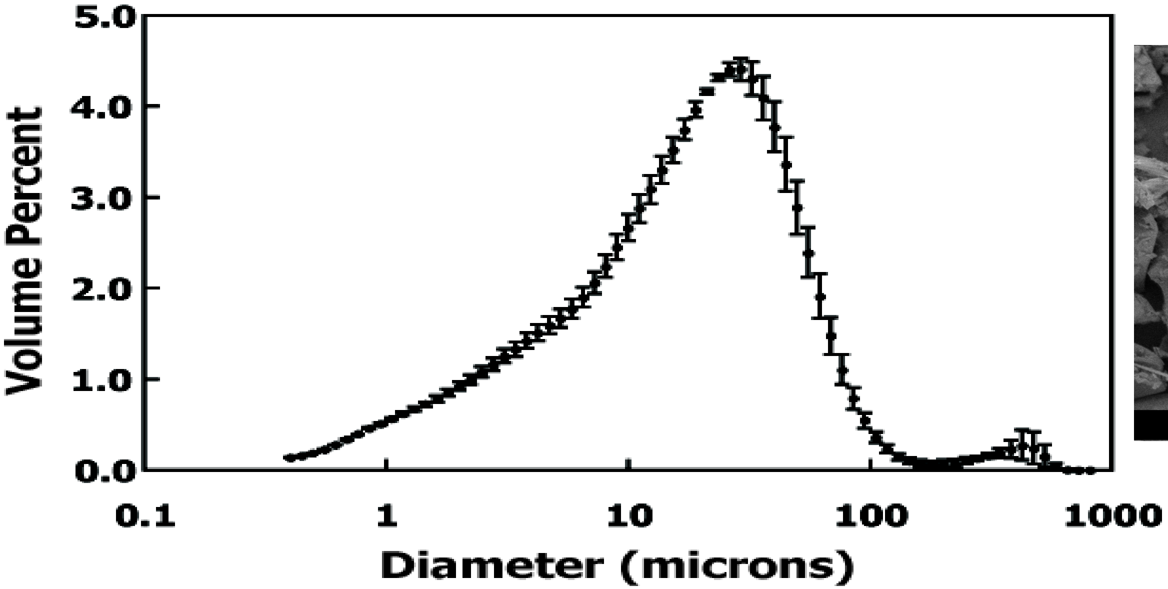

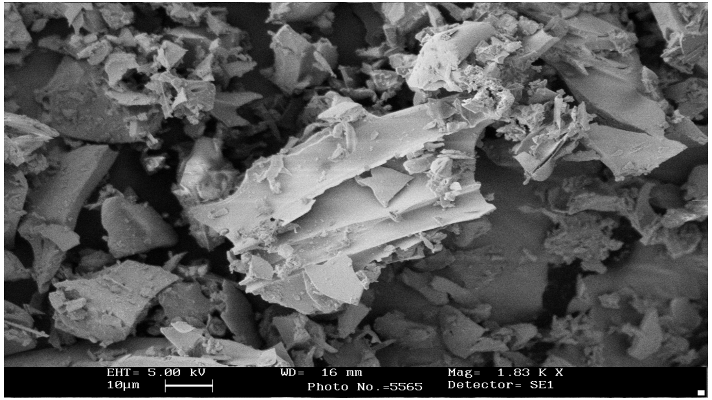

Collisional ash production experiment

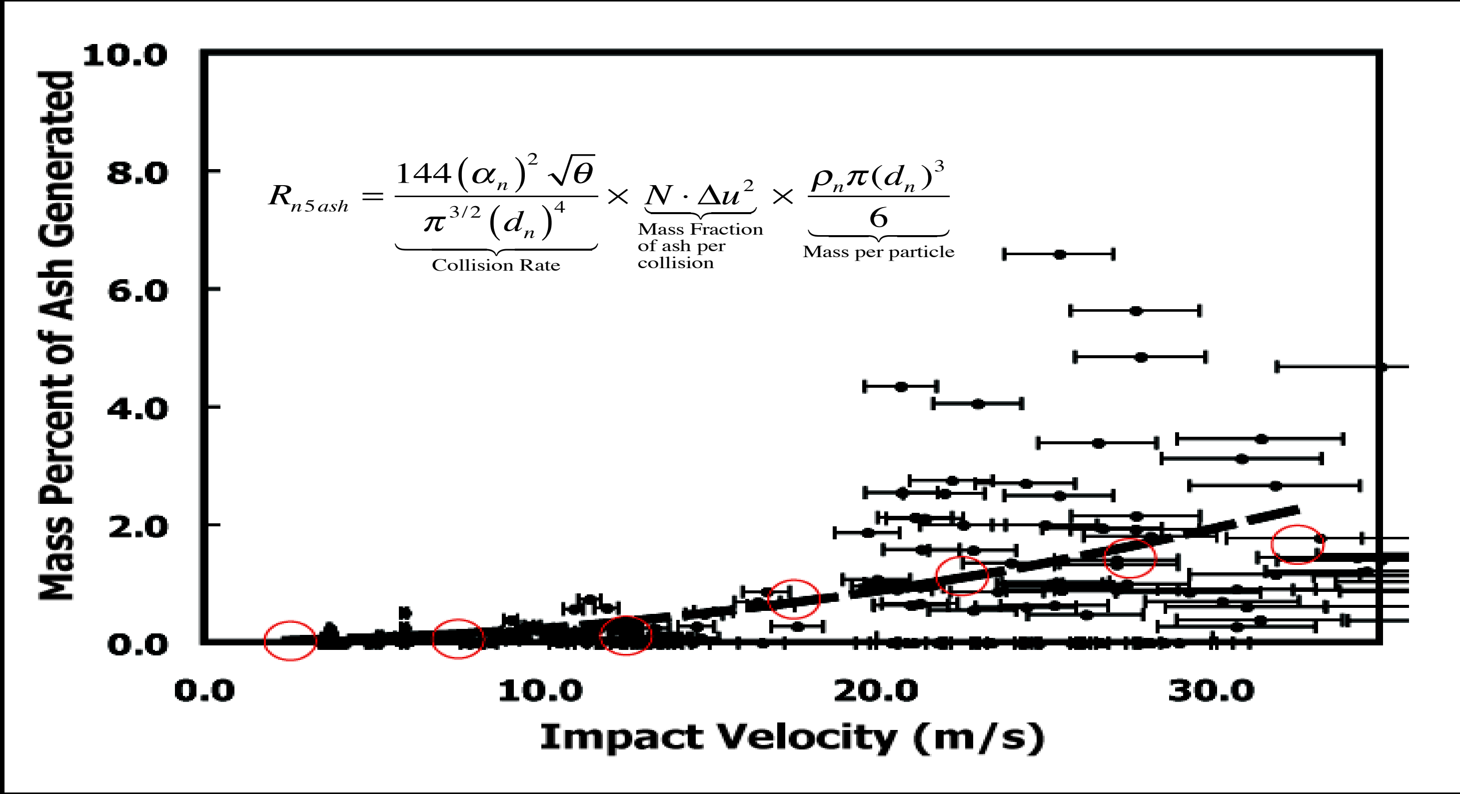

$$R_{n5ash} = \underbrace{\frac{144(\alpha_n)^2\sqrt{\theta}}{\pi^{3/2}(d_n)^4}}_{\text{Collision Rate}} \times \underbrace{N \cdot \Delta u^2}_{\text{Mass Fraction of ash per collision}} \times \underbrace{\frac{\rho_n \pi (d_n)^3}{6}}_{\text{Mass per particle}}$$

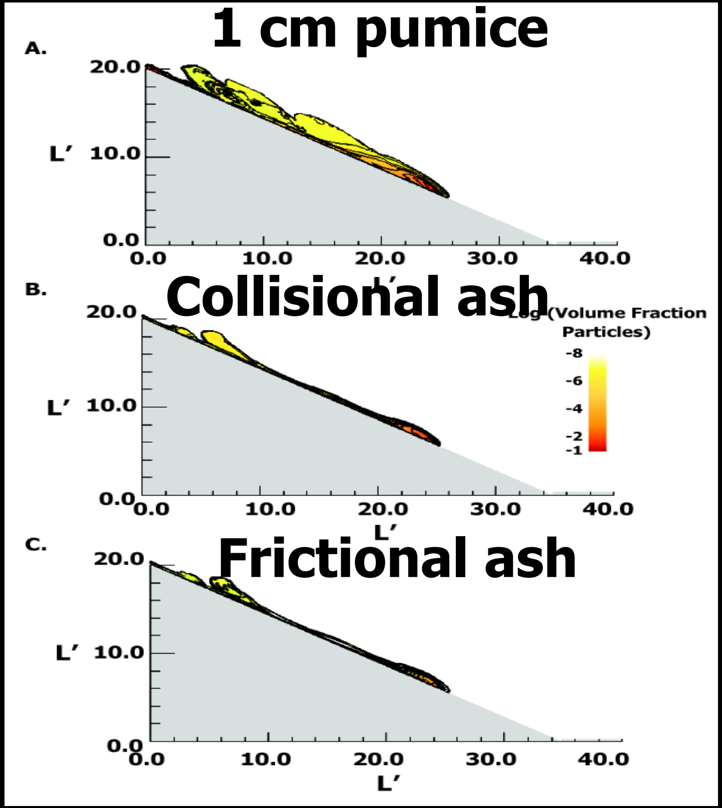

Comminution

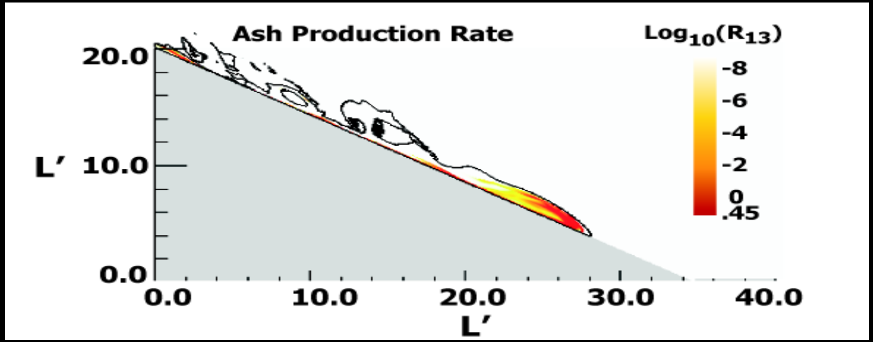

Comminution ash production results in longer runout, enhanced pore pressure and rounded particles.

Dufek and Manga, 2009

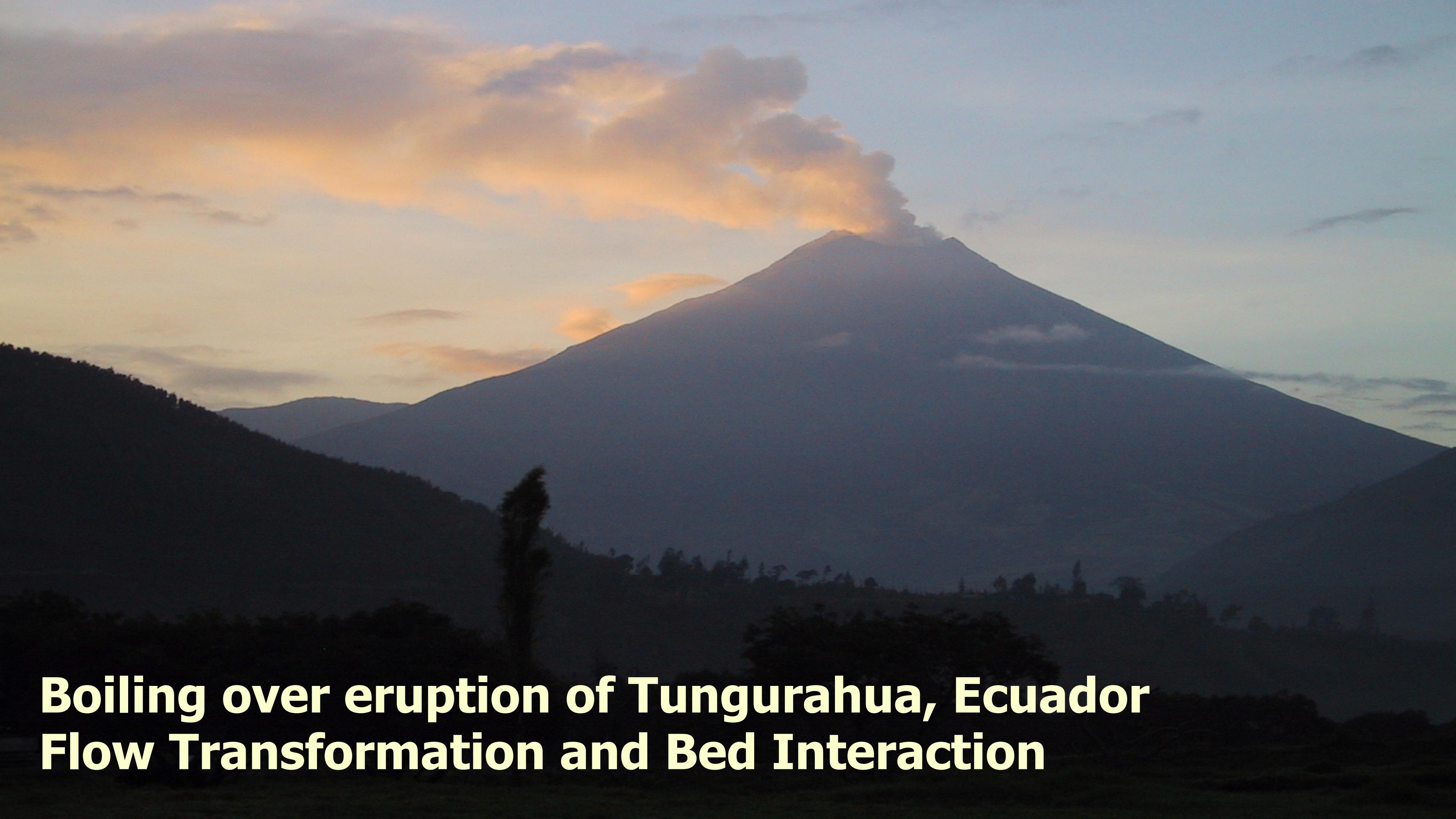
Boiling over eruption of Tungurahua, Ecuador
Flow Transformation and Bed Interaction


July 2006

Tungurahua Pyroclastic Density Currents - 2006

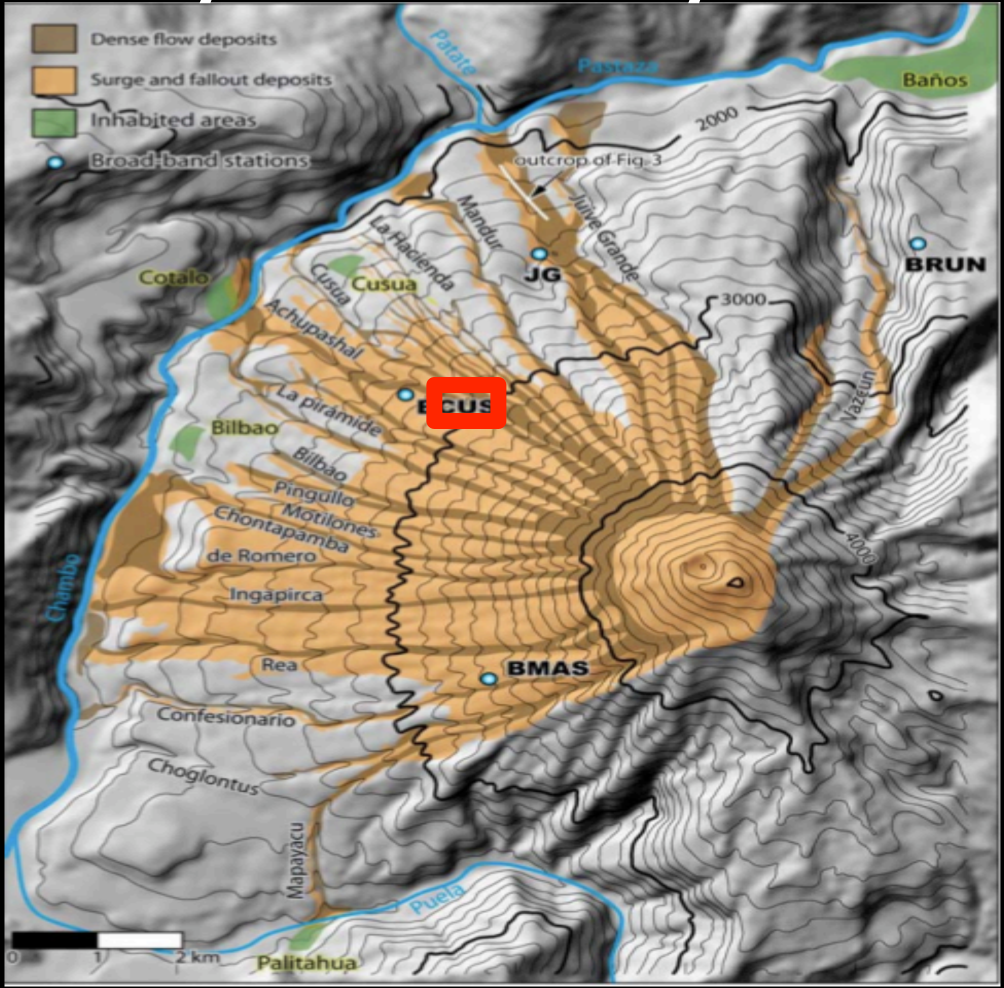

Tungurahua Pyroclastic Density Currents - 2006

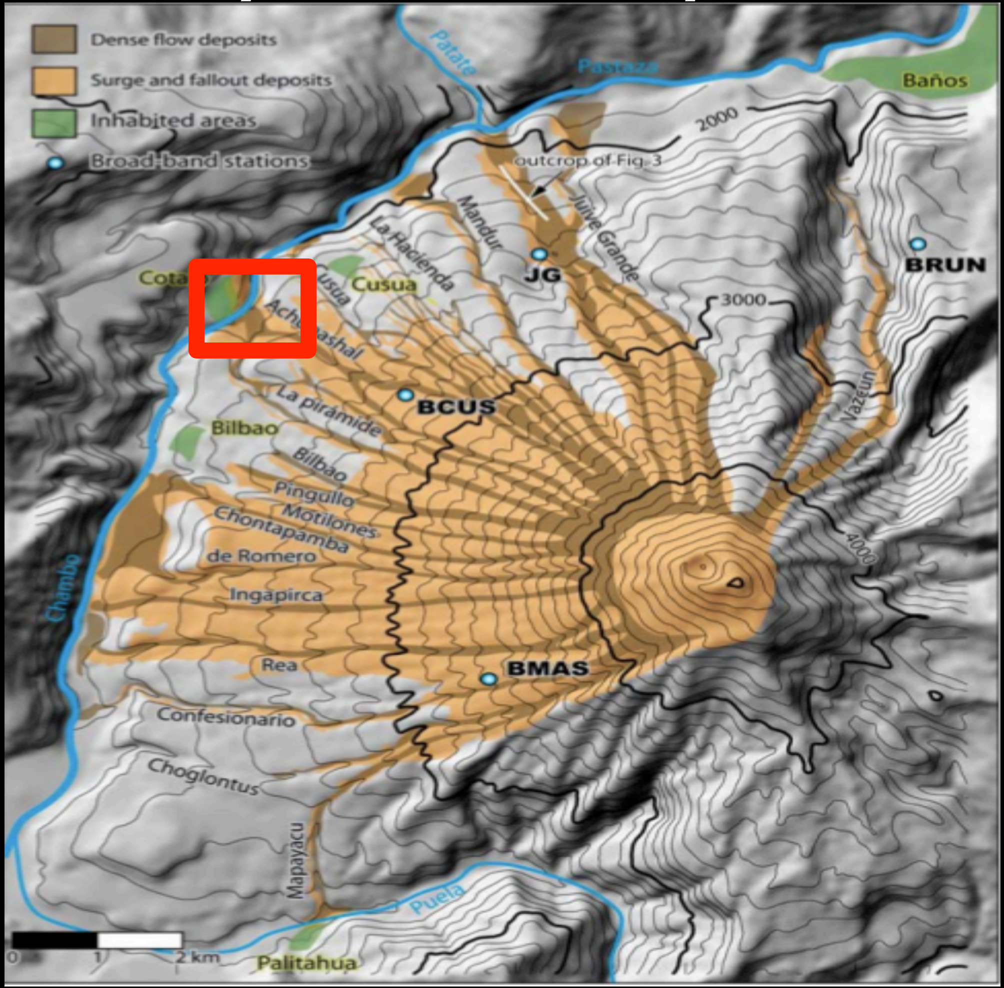

Axes in meters

Simulation of Rio Chambo Encounter

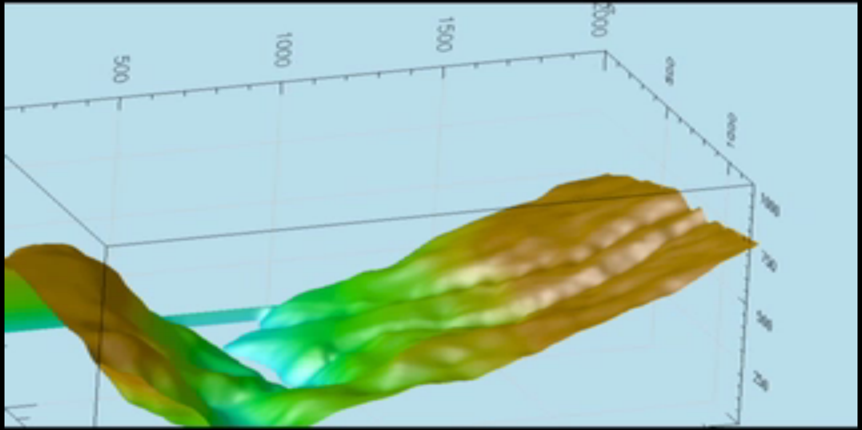

Differential GPS Data

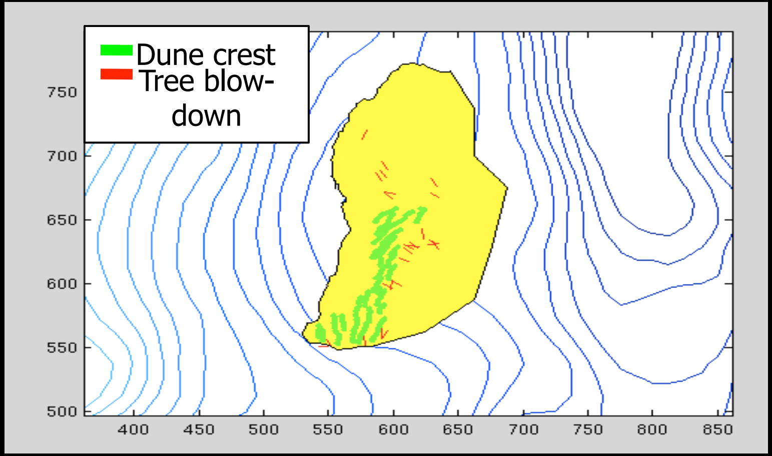

- Transparent Isosurfaces 10^{-2}, 10^{-3} ,10^{-4},10^{-5} Volume Fraction Particles (Except for last sequence, just 10^{-2})

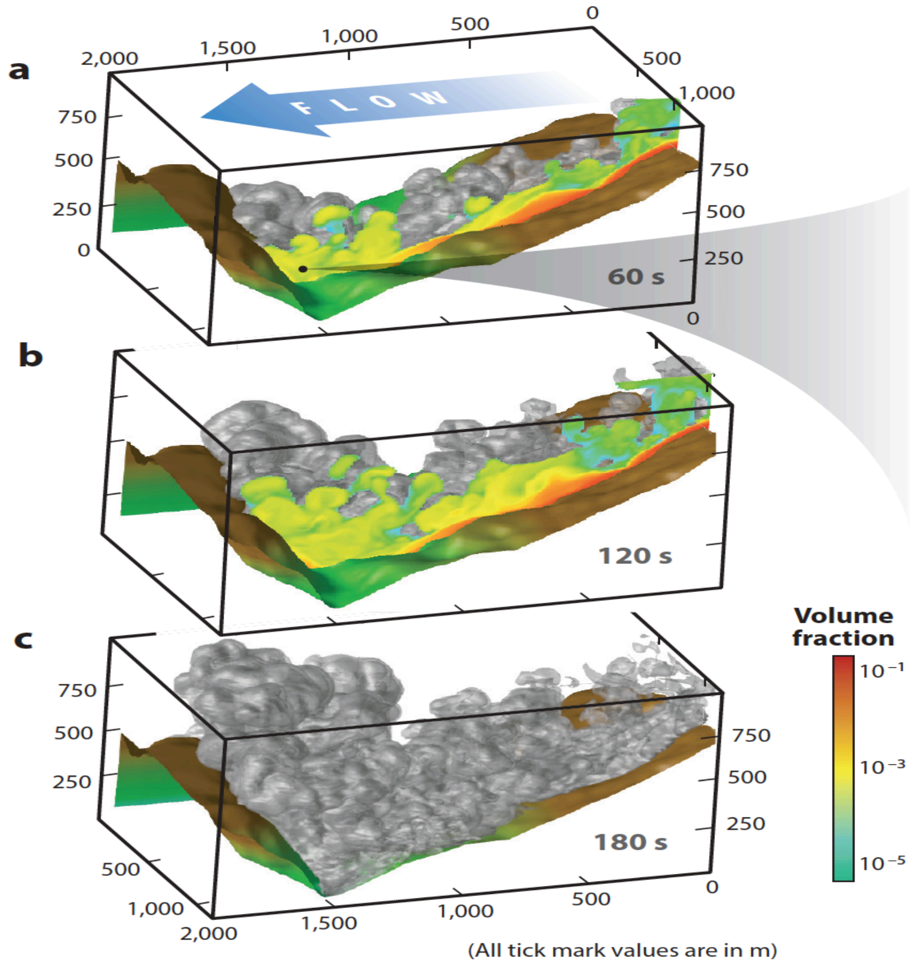

Bed forms:
Tungurahua 2006 eruption, Ecuador

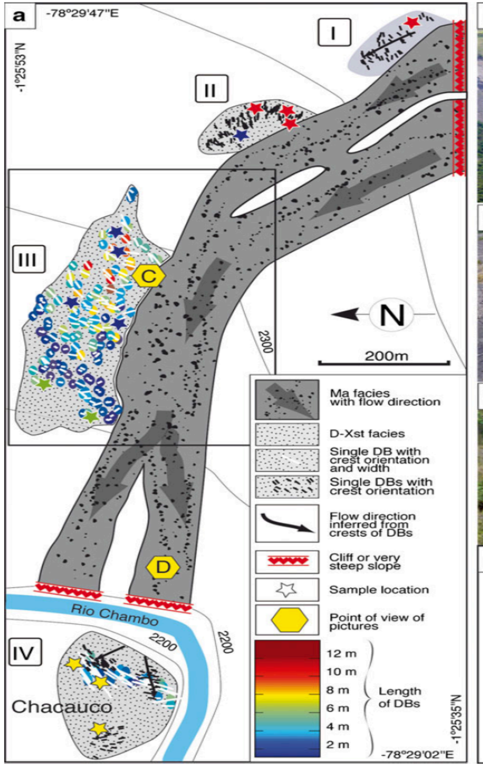

Douillet et al., 2013

Dufek, 2016

Microphysical Model for Rind Thickness

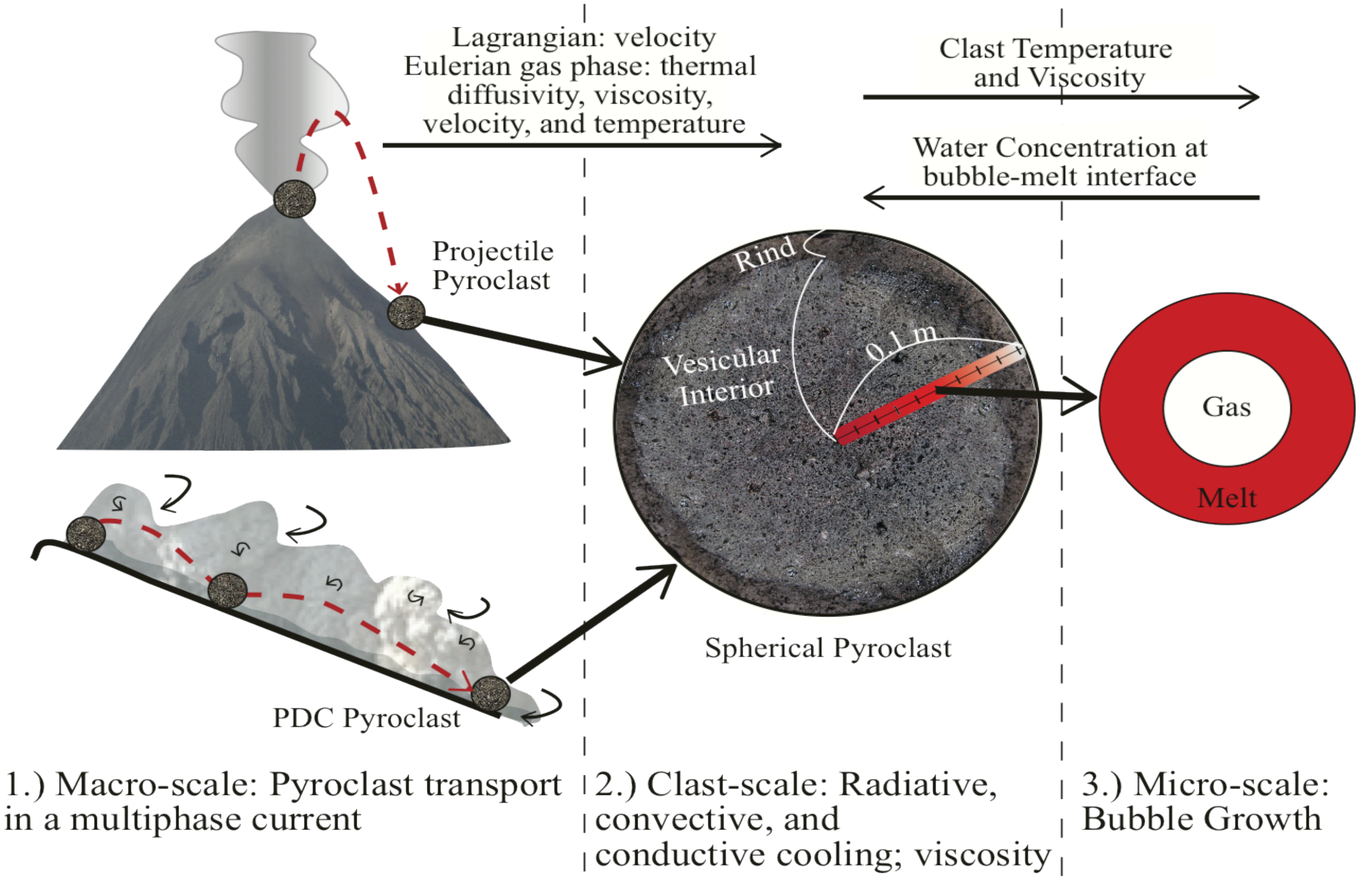

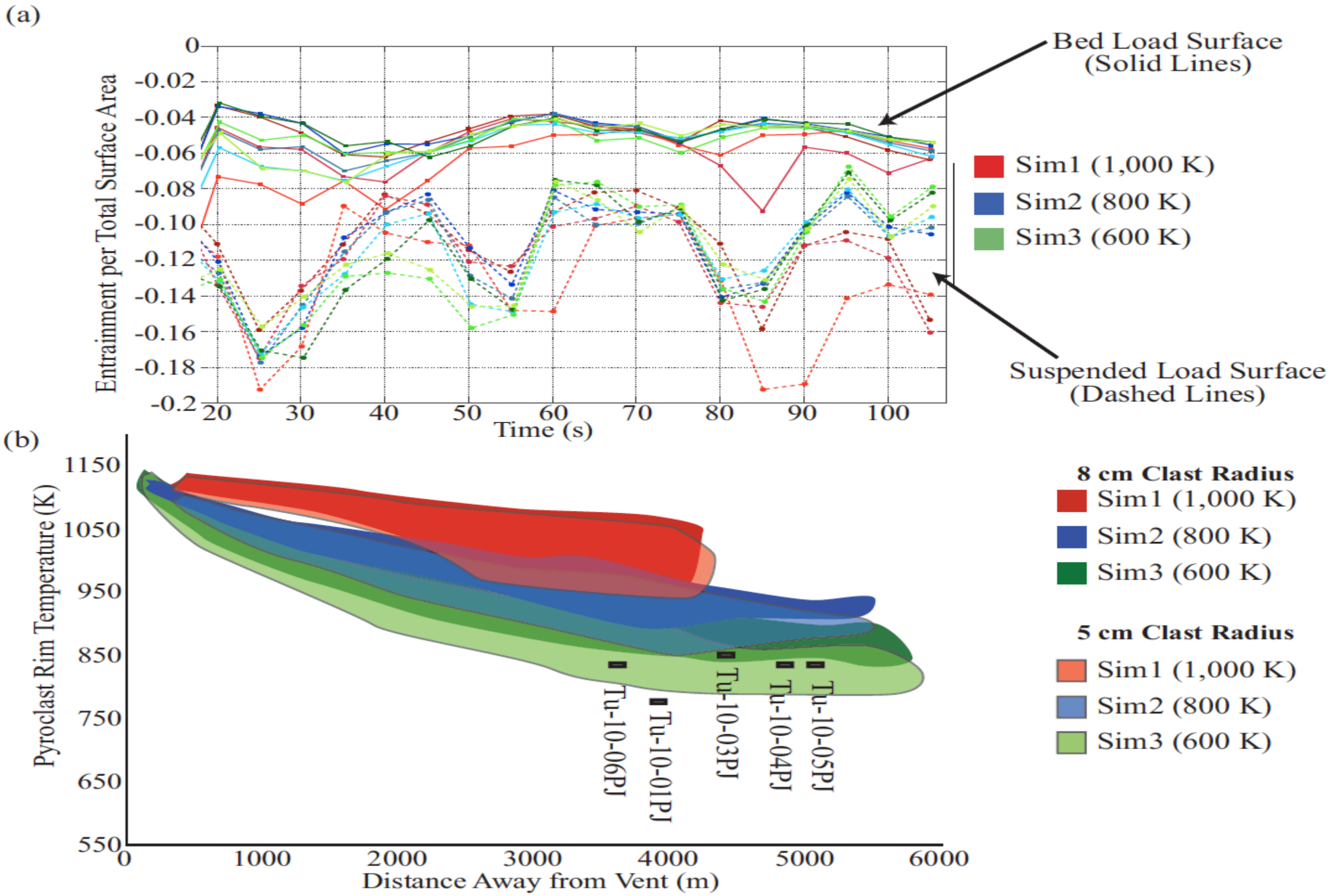

(a)
Entrainment per Total Surface Area
0
-0.02
-0.04
-0.06
-0.08
-0.10
-0.12
-0.14
-0.16
-0.18
-0.2
20
30
40
50
60
70
80
90
100
Time (s)
Bed Load Surface (Solid Lines)
Suspended Load Surface (Dashed Lines)
Sim1 (1,000 K)
Sim2 (800 K)
Sim3 (600 K)
(b)
Pyroclast Rim Temperature (K)
1150
1050
950
850
750
650
550
0
1000
2000
3000
4000
5000
6000
Distance Away from Vent (m)
Tu-10-06PJ
Tu-10-01PJ
Tu-10-03PJ
Tu-10-04PJ
Tu-10-05PJ
8 cm Clast Radius
Sim1 (1,000 K)
Sim2 (800 K)
Sim3 (600 K)
5 cm Clast Radius
Sim1 (1,000 K)
Sim2 (800 K)
Sim3 (600 K)

Bed interaction responsible for erosion (much like other granular flows)

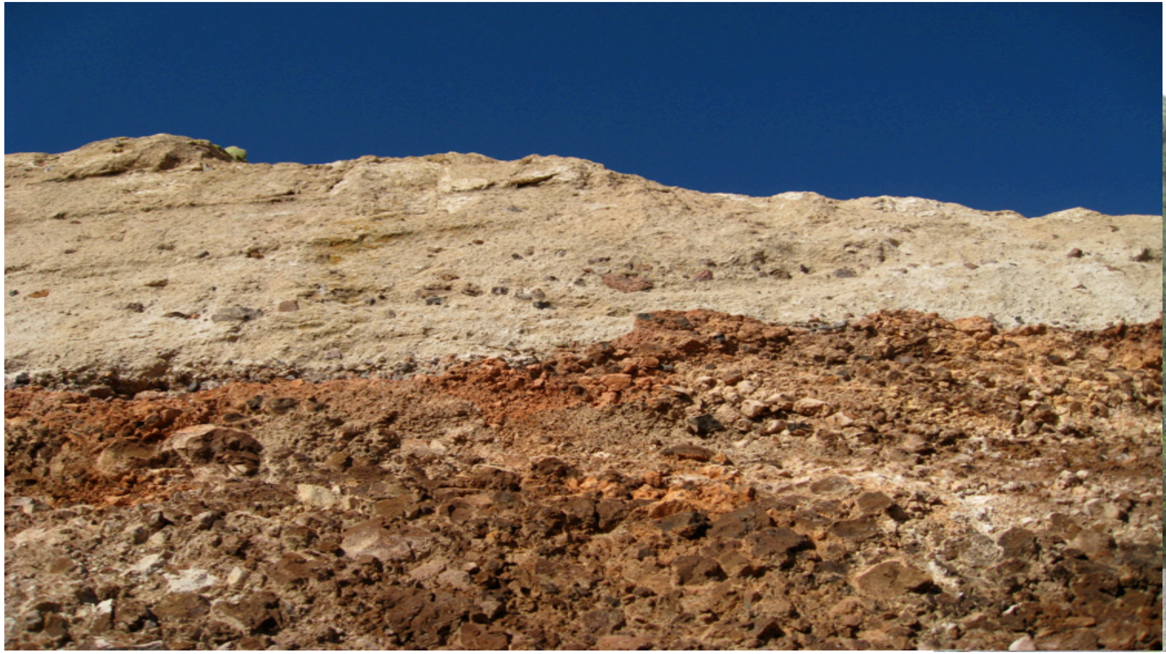

Peach Springs Tuff (AZ)

Tungurahua, Ecuador

Discrete/fluctuating nature of granular flows may play an important role in threshold behavior

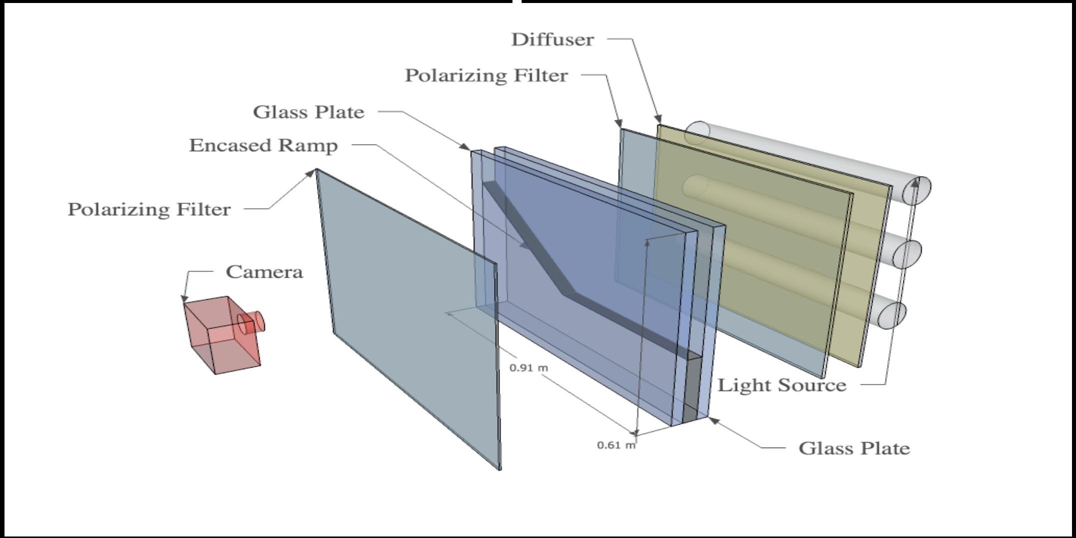

Estep and Dufek, 2012

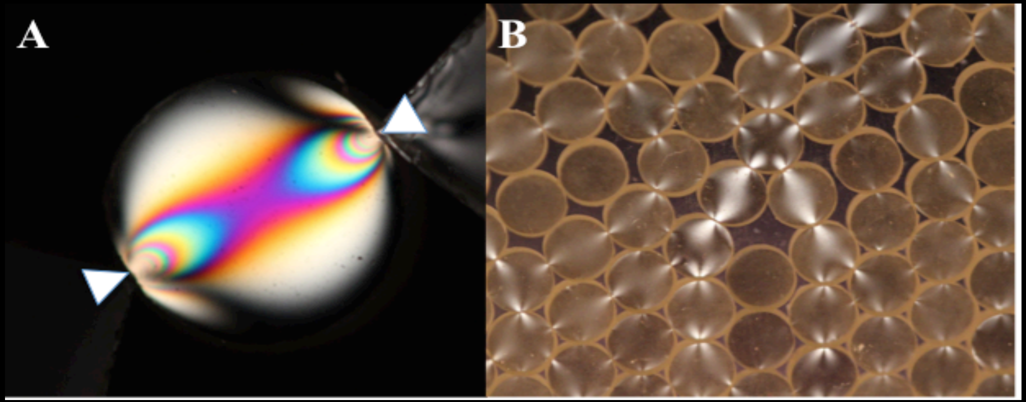

Photoelastic

200 fps

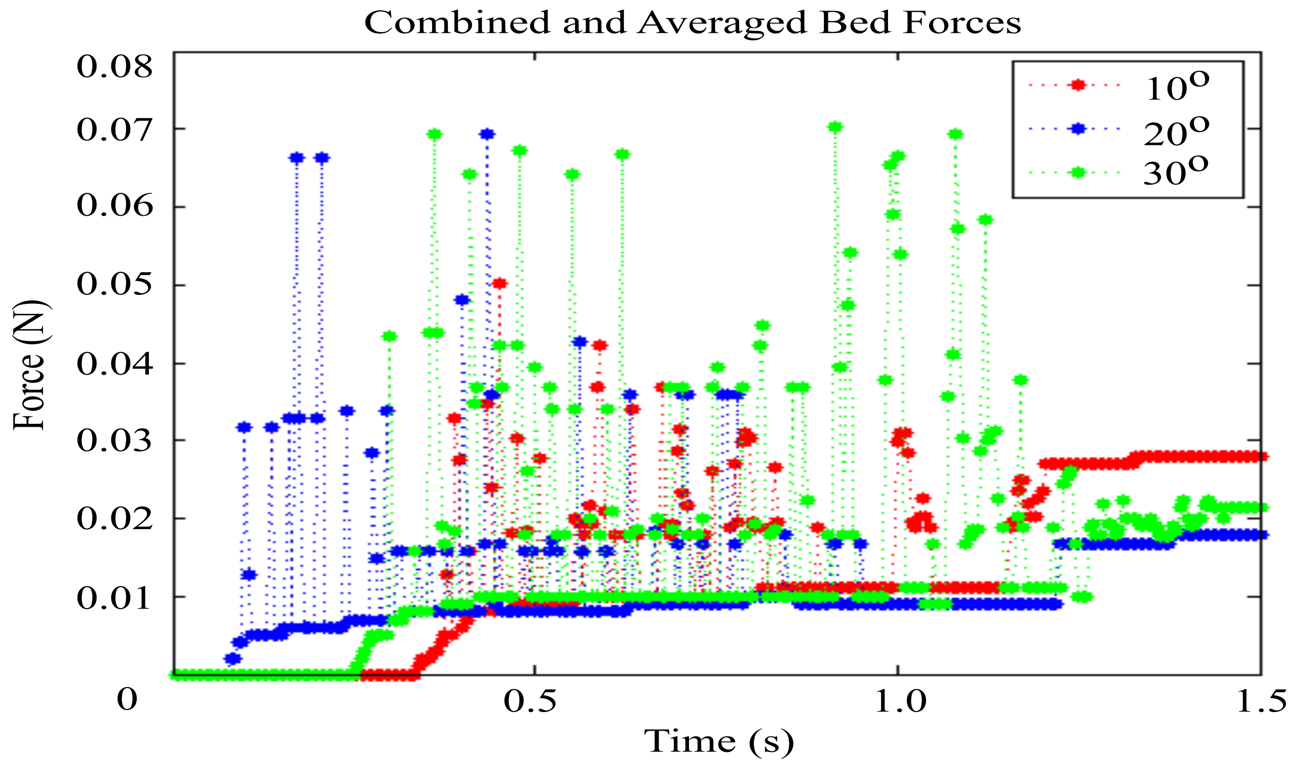

Estep and Dufek, 2012

Some Thoughts on the Challenges and Opportunities in the Study of PDC

1. As gravity currents, much of the dynamics of PDC are modified by processes that change the concentration of the current, including:

    Sedimentation
    Erosion
    Entrainment
    Interaction with topography

All of these processes influence the local particle concentration and momentum transfer mechanisms.

2. Geophysical constraints on PDC are sparse, and future observations of on-going currents to ‘see’ inside these currents would be valuable.

3. Integrating experiments, numerical models, and observations (both real time and deposits) across the range of scales in PDC is needed; this includes advances to examine higher energy dynamics in experimental PDC and to resolve smaller scales numerically.